NATIONAL ADVISORY COMMITTEE FOR AERONAUTICS

TECHNICAL NOTE

No. 1149

PERFORMANCE OF HOODS FOR AIRCRAFT EXHAUST-GAS TURBINES

By L. Richard Turner, Warren H. Lowdermilk
and Albert M. Lord

Aircraft Engine Research Laboratory
Cleveland, Ohio

Washington
November 1946

NATIONAL ADVISORY COMMITTEE FOR AERONAUTICS

TECHNICAL NOTE NO. 1149

PERFORMANCE OF HOODS FOR AIRCRAFT EXHAUST-GAS TURBINES

By L. Richard Turner, Warren H. Lowdermilk
and Albert M. Lord

SUMMARY

The performance of a turbosupercharger turbine was measured
with three types of exhaust hood. The effectiveness of the turbine-
hood combination was determined by measuring the turbine power and
the thrust of the jet discharged from the hood at pressure ratios
across the turbine and hood of 1.35, 1.7, and 2.0 for a range of
blade-to-jet speed ratios from 0.1 to 0.9. Compressed air was used
as the driving fluid.

The results of these tests indicate that an exhaust hood should
have an inlet area equal to the bucket-annulus area of the turbine
and should be equipped with straightening vanes. A system of vanes,
the total chord of which was equal to the turbine pitch-line circum-
ference, achieved complete straightening of the flow. Losses due to
swirl were reduced, however, to about one-half their maximum by
straightening vanes with a total chord 0.175 times the turbine
pitch-line circumference. The flat-nozzle hood, which was designed
to guide the gas from the round bucket-annulus section into a flat
duct, imposed no greater losses than the best conical hood. The
turning of high-velocity flow in a flat duct led to very large
losses. A conventional short-turning-radius hood was found to give
larger losses than the vaned-conical and flat-nozzle hoods.

INTRODUCTION

When a turbosupercharger is operated at rated speed on a recip-
rocating engine, the gases leave the turbine with an axial velocity
of about 700 feet per second. At an airspeed of 375 miles per hour,
a jet power equivalent to about 25 engine horsepower is produced for
each pound of exhaust gas discharged per second at 700 feet per sec-
ond. This power is from 4.5 to 5.0 percent of the engine power
delivered through the propeller. The desirability of so designing

exhaust hoods that the bucket-leaving loss is recovered (for example, for jet propulsion) is obvious. Even with some types of inefficient exhaust hood, an appreciable jet power can be obtained by an increase in exhaust back pressure but this method of operation causes a loss in engine power and also in engine fuel economy. Furthermore, the increased back pressure has an adverse effect on engine-operation limits and on the power for turbine operation in cruising.

The importance of providing efficient exhaust hoods for turbine-compressor jet-propulsion engines is even more obvious as all the power of these units is provided by the discharge of the exhaust gas from the turbine.

An ideal exhaust hood would rearwardly direct the axial momentum of the gas leaving the turbine without loss and would also rearwardly redirect any tangential momentum. An inefficient exhaust hood might, however, destroy the existing momentum and perhaps might require an additional pressure drop to discharge the gases; or the hood might increase the tangential momentum of the jet at the expense of an increased back pressure. Angular momentum remaining in the jet after it is discharged from the hood is not useful for jet propulsion and its existence may reduce the thrust obtainable with a given hood-exit area and a given mass flow.

Very little information is available on the performance of exhaust hoods for aircraft exhaust-gas turbines. Tests were performed at the NACA Cleveland laboratory to compare various hood designs to find their effect on the turbine and hood performance on the basis of the power available to aircraft in flight. Three general types of hood were tested: conical hoods, a flat-nozzle hood, and a short-turning-radius hood of semicircular cross section. Successive modifications were made on the conical hood to determine the sources of the various losses. The results of the tests are presented as curves in terms of generalized parameters.

SYMBOLS

The following symbols are used in the report:

A   area, (sq in.)

F   thrust, (lb)

g   acceleration of gravity, (32.2 ft/sec^2)

H   total pressure, (lb/sq in. absolute)

M mass flow of air, (slugs/sec)

P turbine power, (ft-lb)/(sec)

p static pressure, (lb/sq in. absolute)

R gas constant for air, 53.35 (ft-lb)/(lb)(^{O}R)

r radius, (in.)

T total temperature, (^{O}R)

t static temperature, (^{O}R)

u turbine-wheel pitch-line velocity, (ft/sec)

u_c velocity of discharge calculated from continuity equation, (ft/sec)

u_m effective velocity of discharge as measured by thrust target, (ft/sec)

v theoretical jet velocity, (ft/sec) (computed for a drop in pressure from turbine inlet static pressure to exhaust-hood discharge total pressure)

γ ratio of specific heats of air, 1.400

η over-all turbine efficiency

ρ density, (slugs/cu ft)

Subscripts:

1 station at turbine inlet

2 station at hood exit or at bucket exits when no hood was on turbine

METHODS OF CALCULATION

The losses in a turbine-exhaust hood are the sum of the losses due to skin friction, to throttling, and to separation and swirl in the air stream. An attempt was first made to estimate the losses in the exhaust hoods by a direct measurement of the pressures at the entrance and the exit of the hood. Preliminary tests with hoods

showed that the pressures near the turbine wheel varied markedly
from place to place; an evaluation of the hood losses based on
these measurements would therefore be insufficiently accurate.

A second attempt to evaluate the data used an empirical relation
of turbine power, speed, and inlet pressure to estimate the bucket-
discharge pressure. Negative losses for the hoods were sometimes
obtained from this method, however, when no angular momentum could
possibly have been recovered; therefore, the method was abandoned
because the turbine efficiency was being influenced by the hood
design.

Finally all attempts at separation of hood losses and effects
of the hoods on the turbine performance were abandoned and the anal-
ysis of the test data was based on a set of over-all turbine and hood
performance parameters.

Performance parameters. - In this report the performance of the
hoods is described by comparing the turbine power and mass flow pro-
duced at various wheel speeds for a range of values of the ratio of
the static pressure at the inlet of the turbine to the total pressure
at the hood exit. The static pressure at the turbine inlet was
chosen as the upstream pressure because the effect of exhaust back
pressure on engine power is usually based on static exhaust back
pressure.

In order to generalize the results, the power and the mass flow
are represented by the factors $P \left/ \left(p_1 \sqrt{gRT_1} \right) \right.$ and $\left(M \sqrt{gRT_1} \right) \left/ p_1 \right.$,
which have the dimensions of area, and the wheel speed by the dimen-
sionless factor $u / \sqrt{gRT_1}$. The turbine-hood performance parameters
may be converted to efficiencies (based on turbine inlet static pres-
sure and hood-discharge total pressure) and to blade-to-jet speed
ratios by the following equations:

$$\eta = K \, \frac{P \left/ \left(p_1 \sqrt{gRT_1} \right) \right.}{\left(M \sqrt{gRT_1} \right) \left/ p_1 \right.} \tag{1}$$

and

$$\frac{u}{V} = \sqrt{\frac{K}{2}} \, \frac{u}{\sqrt{gRT_1}} \tag{2}$$

where

$$K = \frac{\gamma - 1}{\gamma \left[1 - \left(\dfrac{H_2}{p_1}\right)^{\frac{\gamma-1}{\gamma}} \right]}$$

and K and $\sqrt{K/2}$ have the following values for the pressure ratios used in the report:

p_1/H_2	K	$\sqrt{K/2}$
2.0	1.590	0.892
1.7	2.003	1.001
1.35	3.477	1.318

For most of the hoods, the discharge velocity and the static pressure were not uniform at the hood exit. Because the hood of a turbosupercharger or other aircraft turbine is intended to generate thrust, the velocity of greatest utility is the average or effective jet velocity u_m defined as the ratio of gross jet thrust to mass flow. The jet thrust was therefore measured directly by a thrust target.

The ratio of the effective jet velocity u_m to the average hood-discharge velocity u_c calculated on the basis of the continuity equation $u_c = M/\rho_2 A_2$ is also shown for each hood. This velocity ratio is given by the equation.

$$\frac{u_m}{u_c} = \frac{\rho_2 A_2 u_m}{M} \tag{3}$$

The density ρ_2 was calculated with the assumption that the pressure was constant and equal to the static pressure measured at the hood exit. All of the velocity components except the average axial velocity u_c were neglected in calculating ρ_2. When the velocity is constant across the hood exit and in an axial direction, the ratio u_m/u_c is unity. A value of this ratio other than unity indicates nonuniformity of the jet velocity or of the static pressure.

The following equation, based on an assumed isentropic conversion of velocity energy to pressure energy and on the neglect of heat losses or gains in the hood, was used to calculate the hood-discharge total pressure H_2

$$\left(\frac{H_2}{p_2}\right)^{\frac{\gamma-1}{\gamma}} = \frac{\frac{2\gamma}{\gamma-1}\,gRT_1 - 2\frac{P}{M}}{\frac{2\gamma}{\gamma-1}\,gRT_1 - 2\frac{P}{M} - u_m^2} \tag{4}$$

The neglect of heat losses or gains in the hood in equation (4) is shown in appendix A to have a negligible effect on the value of the over-all pressure ratio required for a given turbine power and wheel speed.

Turbine calibration. - As a convenient standard of comparison, the performance of the turbine without a hood was measured. The turbine exhausted directly to the atmosphere. The performance was plotted in terms of the factors $P\Big/\left(p_1\,\sqrt{gRT_1}\right)$, $\left(M\,\sqrt{gRT_1}\right)\Big/p_1$, and $u\Big/\sqrt{gRT_1}$, with the difference that the pressure ratio in this case was the ratio of the static pressure at the turbine inlet to the total pressure at the bucket-exit annulus. This performance should be close to the maximum performance obtainable because the discharge pressure is credited with the axial velocity component at the bucket exit and no hood losses occurred. Theoretically, higher performance can be obtained with some hoods at blade-to-jet speed ratios where swirl occurs because the hoods may recover some of the tangential velocity. A hood may also increase the turbine efficiency proper by reducing leakage past the bucket tips.

Equation (5) as derived in appendix B is used to calculate the total pressure at the bucket-exit annulus. The total pressure is based on the bucket-discharge static pressure and the average axial component of velocity of the flow from the buckets.

$$\frac{H_2}{p_2} = \left[\frac{\sqrt{\left(\frac{\gamma}{\gamma-1}\,\frac{p_2 A_2}{M}\right)^2 + \frac{2\gamma}{\gamma-1}\,gRT_1 - 2\frac{P}{M}}}{2\left(\frac{\gamma}{\gamma-1}\,\frac{p_2 A_2}{M}\right)} + \frac{1}{2}\right]^{\frac{\gamma}{\gamma-1}} \tag{5}$$

where p_2 is the average bucket-discharge static pressure, as the turbine had no hood, and A_2 is the bucket-annulus area. A value of 41.5 square inches was used for the bucket-annulus area.

Effect of humidity on density and available energy. - In these tests the working fluid was air at a temperature of about 80° F. At high pressure ratios the work abstraction was sufficient to cool the air below its dew point and occasionally below the freezing point. Visual observation of the wake of the turbine with the hoods removed showed that no visible condensation occurred in the air stream until after the flow left the buckets, although in a few cases a slight amount of frost was seen on the turbine buckets. These observations indicate that little or no energy was liberated by condensation while the air was in the turbine and that the turbine power was therefore not affected by condensation.

Condensation did occur in the hoods. The method of analysis of the test data is shown in appendix A to permit neglect of condensation except in the calculation of the density of the gas at the hood exit. This calculation was based on the assumption that, between the turbine and the hood exit, the mixture attained the equilibrium condition at which the air is saturated with moisture. The method used to calculate the density of the wet air and the corresponding correction to the velocity is described in appendix C.

APPARATUS AND TESTS

The exhaust hoods were tested with a single-stage impulse turbine having a wheel pitch-line diameter of 11.0 inches and a cast nozzle diaphragm. The nozzle angle was 22°, the nozzle area was 10.3 square inches, and the bucket height was 1.20 inches. A schematic diagram of the test setup with a conical hood is shown in figure 1. The turbine was driven by compressed air at a temperature of about 80° F and the power was absorbed by a high-speed hydraulic dynamometer. The air supply was provided by an 8-inch pipe with a transition to an elliptical section at the turbine entrance having an area equivalent to a 6-inch diameter pipe. An A.S.M.E. thin-plate orifice was installed in the air-supply pipe upstream of the air-flow control valve.

The air was discharged from the hood into the thrust target, which in turn discharged to the atmosphere. The pressure drop through the target never exceeded 4 inches of water. The target is

similar to that described in reference 1. The thrust, or reaction
of turning the air through an angle of 90°, was measured by a beam
scale. The target consists of a sleeve closed at one end and mounted
to pivot about an axis at right angles to the direction of discharge
of the air from the sleeve. The sleeve was mounted inside a tank.
The air entered the sleeve through a hole near the closed end and was
turned through an angle of 90°. When the axis of support of the
sleeve is normal to the direction of the flow of the air as it enters
the target, the moment of momentum produced is equal to the product
of the momentum of the air stream times its mean distance from the
supporting axis. The distance from the center of the entering air
stream to the axis of support of the sleeve and the length of the
reaction arm are equal; the scale therefore reads the jet thrust.

Calibration of thrust target. - The thrust target was calibrated
by measuring the reaction of an air jet flowing axially from a noz-
zle. The thrust of the air jet was determined by making a wake sur-
vey of the nozzle. A comparison of the jet thrust as measured by the
target and by the nozzle wake survey is shown in figure 2. The dif-
ferences are small.

Turbine calibration. - The turbine first was calibrated as a
reference using a fairing post to stablize the air flow from the
wheel. (See fig. 3.) The static pressure at the wheel exit was
assumed to be the average of the pressure measured on the fairing
post and the barometric pressure.

Types of hood. - The types of hood tested were:

1. Conical hood with the following modifications:

(a) Long-chord straightening vanes and wheel fairing (fig. 4(a))

(b) Long-chord vanes, wheel fairing, and hood-entrance fairing
band (fig. 5(a))

(c) Wheel fairing supported by 3/8-inch tubes (fig. 6(a))

(d) Plain conical hood (fig. 7(a))

(e) Flat cooling cap and short-chord straightening vanes
(fig. 8(a))

(f) Flat cooling cap supported by 3/8-inch tubes (fig. 9(a))

(g) Conventional cooling cap (fig. 10(a))

2. Flat-nozzle hood with two extensions:

(a) Straight extension (fig. 11(a))

(b) 90° bend extension (fig. 12(a))

3. Short-turning-radius hood (fig. 13(a))

The hood-exit areas of types 1, 2, and 3 were 29.0, 43.5, and 53.4 square inches, respectively.

Measurements. - The following measurements were made:

Turbine inlet static pressure

Turbine inlet total temperature

Air flow

Turbine-wheel speed

Turbine torque

Thrust

Hood-discharge static pressure

Static pressure on wheel fairing post (measured only during turbine calibration)

RESULTS AND DISCUSSION

The calibration of the turbine with the wheel fairing post is shown in figure 3. Figure 3(a) shows a diagram of the wheel and the fairing post; figure 3(b) shows the power factor and mass-flow factor for the turbine. The ratio of the blade speed to the theoretical jet speed u/v based on the over-all pressure ratio p_1/H_2 is shown for reference.

Conical Hoods

Conical hood with long-chord straightening vanes and wheel fairing. - The performance characteristics of the turbine and hood with a conical wheel fairing and two long-chord straightening vanes

are shown in figure 4. A drawing of the hood is shown in figure 4(a).
The power and mass-flow factors are shown in figure 4(b).

At a pressure ratio of 1.35, the turbine power with the hood is
equal to the turbine power measured during the turbine calibration
but the mass flow is slightly reduced (fig. 3(b)). As compared with
the turbine calibration the over-all efficiency computed from equa-
tion (1) is increased about 1.4 points (from 68.4 to 69.8 percent).
At a pressure ratio of 1.7, the turbine power and mass-flow factors
are equal to those measured during the turbine calibration except at
very high wheel speeds. Then the mass flow and power are reduced,
apparently because of large hood losses. The over-all turbine-hood
efficiency is lower than that for the turbine calibration in this
high-wheel-speed region. At a pressure ratio of 2.0, a loss in power
occurs as compared with the turbine calibration (fig. 3(b)), with
the hood corresponding to about 2 points of turbine efficiency.

The ratio of the effective hood-discharge velocity u_m (as
measured by the thrust target) to the hood-discharge velocity u_c
calculated from the continuity equation is shown in figure 4(c).
The value of this ratio is substantially constant over the turbine-
speed range and nearly equal to unity in agreement with the obser-
vation, made with the target removed, that the flow from the hood
was substantially axial and uniform at all times.

The jet velocity calculated from the continuity equation may
differ from the effective velocity for two reasons: (a) When the
average pressure in the hood exit is equal to the discharge pressure
measured at the rim of the hood, the velocity calculated from the
continuity equation will be less than the effective velocity if the
velocity profile is not flat; (b) if the velocity components are not
parallel to the axis of the hood, the static pressure is not uniform
and, in general, the average pressure is not equal to the discharge
pressure. In this case the calculated velocity u_c may not equal u_m
because u_m is based on the thrust-target measurement, which includes
the integrated effect of the pressure variation, whereas the calcu-
lated value u_c is the axial component of only the velocity. The
effective velocity u_m can be greater or less than the calculated
velocity u_c depending on whether the average static pressure is
greater or less than the free-air static pressure p_2 at the hood
exit.

The values of u_m/u_c in figure 4(c) less than unity are thus
probably due to the existence of low-pressure areas in the hood
exit.

Conical hood with long-chord straightening vanes, wheel fairing, and hood entrance fairing band. - The previously mentioned conical hood (fig. 4(a)) did not provide a smooth and close-fitting entrance for the passage of air from the buckets to the hood. In order to determine the possibility of reducing the losses in this region, tests were run with a fairing band installed in the hood entrance. (See fig. 5(a).) This fairing band made the hood-entrance area equal to the bucket-annulus area.

The power and the mass flow obtained with this hood are shown in figure 5(b). The principal effect of the fairing was to increase the power at every point. The improvement attained is equivalent to about 1 point in turbine efficiency. The velocity ratio u_m/u_c is shown in figure 5(c). The variation is similar to that of the vaned conical hood without the fairing band (fig. 4(c)).

Conical hood with wheel fairing supported by 3/8-inch diameter tubes. - In order to determine the value of straightening vanes in conical hoods, tests were run with a conical hood (fig. 6(a)) similar to the vaned conical hood, figure 4(a), except that no straightening vanes were used. The wheel fairing was supported by six 3/8-inch-diameter tubes.

The power and mass-flow factors for this hood are shown in figure 6(b). At wheel speeds equivalent to a blade-to-jet speed ratio of approximately 0.4, the power obtained is only slightly less than the power for the vaned hood with the entrance fairing band. The loss at much higher or lower wheel speeds was very great. No recovery of tangential momentum was obtained under any condition. The pressure loss was so great that the turbine could not be operated at a rotative speed appreciably greater than that for axial flow from the buckets. Axial flow occurs at a wheel speed approximately 10 percent lower than the wheel speed for maximum power output with the efficient hoods such as the vaned conical hoods (figs. 4(b) and 5(b)).

The high loss of power was due to swirl in the hood. When an appreciable swirl exists at the bucket exit, the tangential velocity at the hood exit must be very large to maintain the conservation of angular momentum, because the diameter of the hood exit is much smaller than the pitch-line diameter of the turbine wheel. The production of this tangential velocity requires a large drop in static pressure. Any pressure drop used to produce tangential velocity is wasted because angular momentum is not useful for jet propulsion. The total hood-discharge pressure is defined as the pressure that

would produce the effective axial velocity u_m. The power of turbines with vaneless hoods for a constant ratio of the inlet static pressure to total hood-discharge pressure is therefore unusually low when an appreciable part of the available pressure drop is expended in the generation of increased swirl. The long-chord straightening vanes in the conical hood (figs. 4(a) and 5(a)) prevented the growth of swirl.

Losses due to swirl in the vaneless conical hood are more serious for wheel speeds greater than those for axial flow than for wheel speeds less than those for axial flow. The pressure loss is principally determined by the amount of swirl. The hood losses increase the bucket-discharge pressure and thus reduce the speed of the jet approaching the turbine buckets, increase the actual blade-to-jet speed ratio, and decrease the available turbine power. When the wheel speed is increased above the wheel speed for axial flow, the actual blade-to-jet speed ratio and therefore the swirl and the losses rapidly increase because the jet speed decreases as the wheel speed increases. When the wheel speed is decreased below the wheel speed for axial flow, the swirl and the losses increase less rapidly than in the previous case because the true jet speed is decreased as the wheel speed is decreased and the true blade-to-jet speed ratio therefore changes less rapidly.

The variation of the velocity ratio u_m/u_c with blade-to-jet speed ratio u/v is shown in figure 6(c). For nearly axial flow (u/v approximately equal to 0.35 to 0.40), the velocity ratio is nearly unity or equal to that for the vaned conical hood. When the blade-to-jet speed ratio is slightly lower or higher than that for axial flow, the velocity ratio is decreased because of the swirl that exists in the hood. When swirl is present, a radial pressure gradient exists across the exit section of the hood. When the amount of swirl is small the jet completely fills the nozzle; the true axial velocity of the jet is increased by the presence of the low-pressure low-density region near the axis of the nozzle. The momentum of the air discharged from the hood is, however, decreased because momentum can be evaluated only as though each element of the fluid has been brought to atmospheric pressure by a suitable change in its axial velocity. The effective velocity of the central filaments is therefore small because the pressure is low near the axis of the nozzle.

As the amount of swirl is increased the velocity ratio u_m/u_c decreases to a minimum and then increases rapidly. This rapid increase in u_m/u_c is caused by the formation of an annular jet with a stagnant core within the nozzle. Because the flow area is

decreased by the presence of the stagnant core the axial velocity
is increased. In addition, when the jet is hollow the inner edge
is substantially at atmospheric pressure and the average pressure
of the jet is increased by the swirl, which causes a further
increase in the effective jet velocity.

Plain conical hood. - It had been suggested that wheel fairings
and cooling caps had negligible effects on the flow through the
hood of a turbosupercharger. A hood consisting of only the outer
cowling (fig. 7(a)) therefore was tested. The turbine power and
mass-flow factors are shown in figure 7(b). The turbine power was
slightly reduced at every point as compared with the vaneless coni-
cal hood with the wheel fairing (fig. 6(b)). The power loss was
large compared with the losses of the hoods with straightening vanes
(figs. 4(b) and 5(b)) except for nearly axial flow. The net loss
for axial flow corresponds to a loss of from 2 to 3 points in tur-
bine efficiency compared with the conical hood with the long-chord
straightening vanes and entrance fairing band.

The variation of the velocity ratio u_m/u_c with blade-to-jet
speed ratio u/v for this hood, shown in figure 7(c), is similar
to that for the conical hood with the wheel fairing (fig. 6(c)).

A wake survey was made of the flow from this hood in order to
check the accuracy of the thrust-target measurements when the flow
has an appreciable swirl. The results of these measurements, taken
at a turbine-hood pressure ratio p_1/H_2 of 1.35, are shown in
figure 7(d). The dashed curves are taken from figures 7(b) and 7(c)
for a pressure ratio of 1.35.

The agreement between the results obtained with the thrust
target and by means of the wake survey is good except for one point
at the highest wheel speed of the survey, for which the mass flow
and the thrust calculated from the wake survey were appreciably less
than those measured with the target in place. The mass flow calcu-
lated from the wake survey was 11 percent lower than the mass flow
measured with the A.S.M.E. thin-plate orifice during the wake survey.
A considerable error is apparently introduced into the wake-survey
measurements when the tangential velocity is large as compared with
the axial velocity. A method of evaluation of the wake survey of a
flow with swirl about the axis of symmetry is discussed in appendix D.

Conical hood with flat cooling cap and short-chord straightening
vanes. - A flat cooling cap was installed in the entrance of the con-
ical hood immediately behind the turbine wheel and was supported by

three short-chord streamline struts (fig. 8(a)). The chord of each
strut is 2.0 inches. The turbine power for this arrangement is
shown in figure 8(b). As compared with the vaneless hood with no
cooling cap (fig. 7(a)), the power was much greater especially at
high wheel speeds. The power was always less than the power obtained
with the long-chord straightening-vaned hood (fig. 5(b)). A part of
this loss was undoubtedly throttling loss due to the change in area
immediately behind the cooling cap.

Variation of the ratio of the effective hood-discharge velocity
to the calculated hood-discharge velocity u_m/u_c with blade-to-jet
speed ratio u/v is shown in figure 8(c). This figure shows evi-
dence of existence of a considerable swirl in the jet, when compared
with the same ratios for the hood with the long-chord straightening
vanes (fig. 4(c)). The rate of reduction of the velocity ratio
u_m/u_c, as the wheel speed is changed from that for axial flow, is
much less than that obtained with the vaneless conical hood with or
without a wheel fairing (figs. 6(c) and 7(c)) indicating that an
appreciable straightening of the flow had been achieved by the three
short-chord vanes.

Conical hood with flat cooling cap supported by 3/8-inch tubes. -
In order to distinguish between the straightening effect of the small
streamlined struts and any effects directly attributable to the pres-
ence of the flat cooling cap, 3/8-inch-diameter tubes were substituted
for the short-chord, streamlined struts. (See fig. 9(a).) The
turbine-power factor for this condition is shown in figure 9(b).
The losses are equal to those for the vaneless conical hood with no
cooling cap (fig. 7(b)). The small streamlined struts previously
used to support the cooling cap therefore apparently effected an
appreciable reduction in swirl; whereas the round struts had no
noticeable effect.

The variation of the velocity ratio u_m/u_c with blade-to-jet
speed ratio u/v, shown in figure 9(c), is similar to that for the
vaneless conical hood.

A comparison of figures 6, 7, 8, and 9 with figure 5 shows that
maximum power and therefore maximum efficiency were normally obtained
at a wheel speed somewhat greater than that for axial flow from the
turbine buckets.

Conical hood with conventional cooling cap. - The turbine power
for the conical hood with a conventional cooling cap (fig. 10(a)) is
shown in figure 10(b). The loss of power is greater than that for

the flat cooling cap supported by three short-chord vanes (fig. 8) under all conditions. The maximum over-all efficiency is decreased about 3 to 4 points as compared with the increases in efficiency given by the hoods of figures 4(b) and 5(b). Although some straightening of the flow was attained with the elliptical vanes, the vanes were either too large in diameter or too poorly streamlined to provide a flow path with low average resistance.

The variation of the velocity ratio u_m/u_c with blade-to-jet speed ratio u/v shown in figure 10(c) is similar to that for the conical hood with the short-chord struts (fig. 8(c)). The formation of a pronounced hollow-cored jet from the hood did not occur with either the short-chord streamlined vanes or with the conventional cooling cap as evidenced by the fact that the velocity ratio did not tend to rise at the high and low blade-to-jet speed ratios. This behavior indicates that the flow remained more nearly uniform than in the case of the vaneless hood (fig. 7(c)).

Flat-Nozzle Hoods

The flat-nozzle hood (figs. 11(a) and 11(b)) was so designed that the entrance area was equal to the bucket-annulus area. It was also designed to bring the gas from the round annulus section into a flat duct. The flow passages midway between the straightening vanes were chosen to give minimum friction and turning losses. The air flowing from the wheel near the vanes followed a nearly straight path when the flow from the buckets was in an axial direction.

Flat-nozzle hood with straight extension. - The turbine power and mass-flow factors for the flat-nozzle hood with a straight extension are shown in figure 11(b). The maximum power output was slightly less than that of the turbine with the best conical hood (fig. 5) compared at the same pressure ratios.

The flat-nozzle hood, however, reduced the mass flow enough that the over-all efficiency was about 1 point higher than that for the best conical hood at a pressure ratio of 2.0. At the pressure ratios of 1.35 and 1.7 the efficiency was equal to that for the best conical hood (fig. 5(b)).

The velocity ratio u_m/u_c for the flat hood with the straight extension is shown in figure 11(c). The velocity ratio was greater than unity for all conditions, indicating that the flow was always nonuniform. Observation of the flow with the thrust target removed showed a distinct nonuniformity of the flow for all pressure ratios and wheel speeds.

Flat-nozzle hood with 90°. bend extension. - A 90° bend exten-
sion with the radius of curvature of the bend equal to the width of
the hood extension was tested with the flat-nozzle hood. (See
fig. 12(a).) The power and mass-flow factors for this hood and
extension are shown in figure 12(b). At the pressure ratios of 1.35
and 1.7, the power factor for the 90° bend extension is nearly equal
to that for the straight extension. At the pressure ratio of 2.0, a
serious loss occurs. The velocity u_m/u_c for the flat-nozzle hood
with 90° bend is shown in figure 12(c). The high peak of this ratio
and the poor over-all performance of this hood at a pressure ratio
of 2.0 are probably the result of the formation of a stable system
of shock waves at the downstream end of the bend.

Short-Turning-Radius Hood

A sketch of the conventional short-turning-radius hood is
shown in figure 13(a). The power and mass-flow factors for this
hood are shown in figure 13(b). The maximum power factor of this
turbine-hood combination is about 11.5 percent lower than the power
factor for the conical hood with long-chord straightening vanes and
hood-entrance fairing band (fig. 5).

The power and mass-flow factors for this hood decrease less
rapidly as the turbine speed increases above the wheel speed for
axial flow than for the conical hoods, which indicates that the
short-turning-radius hood is able to recover a part of the residual
swirl under some conditions.

The velocity ratio u_m/u_c for the short-turning-radius hood
is shown in figure 13(c). The velocity ratio shows a pronounced
rise at high wheel speeds.

Comparison of Performance of Various Hoods by

Means of Turbine Torque Coefficient

Turbine data may conveniently be represented by a plot of the
torque coefficient

$$\frac{\eta}{2(u/v)} + \frac{u}{v}$$

against the wheel-speed parameter $u/\sqrt{gRT_1}$ or the blade-to-jet speed ratio u/v. At a fixed value of u/v, or of $u/\sqrt{gRT_1}$, the changes in the torque coefficient are proportional to changes in the efficiency. Because the efficiency is divided by u/v, the torque coefficient varies more rapidly with losses than does the efficiency. The usual method of plotting efficiency or power against wheel speed u or against u/v tends to mask the effect of losses in the region of low wheel speeds and to enlarge them at high wheel speeds.

The relation between torque coefficient and the wheel-speed parameter at a pressure ratio of 2.0 is shown in figure 14 for the turbine without a hood and for the hoods described in figures 5, 6, 8, 11, and 13. The difference in the values of torque coefficient for the several exhaust configurations is an indication of the differences in efficiency.

The three short-chord streamlined struts (having a solidity of 0.175, where solidity is defined as the total chord length divided by the turbine pitch-line circumference) effected about one-half as great an improvement in performance as the long-chord strut, which had a solidity of 1.0. This result suggests than an intermediate straightening-vane solidity may be adequate for most applications. The solidity of the straightening vanes in the flat hood (0.335) was apparently adequate to straighten the flow in a hood of non-conical form.

SUMMARY OF RESULTS

From tests of turbine-hood combinations with compressed air as the working fluid, the following results were obtained:

1. Throttling and leakage losses were reduced by the use of a hood having a flow area at the hood entrance equal to the bucket-annulus area as compared with a hood having a larger entrance area.

2. Straightening vanes were necessary to avoid large losses due to swirl when the turbine equipped with a conical hood was operated with residual swirl in the fluid leaving the turbine wheel.

3. Practically complete straightening of the flow was achieved by straightening vanes with the total chords equal to the turbine

pitch-line circumference. Losses due to swirl were reduced, however, to about one-half their maximum by straightening vanes with a total chord 0.175 times the pitch-line circumference of the turbine.

4. The flat-nozzle hood, which was designed to guide the gas from the round bucket-annulus section into a flat duct, imposed no greater loss than the best conical hood. At high Mach numbers, the losses in a 90° bend, high-aspect-ratio, flat duct with the axis of bending parallel to the longer side were very large.

5. The conventional short-turning-radius hood often used for a flight hood in turbosupercharger installations gave 11.5 percent less power than the conical hood with long-chord straightening vanes and hood-entrance fairing band at a blade-to-jet speed ratio of 0.4 and a pressure ratio of 2.0.

Aircraft Engine Research Laboratory,
    National Advisory Committee for Aeronautics,
        Cleveland, Ohio, May 27, 1946.

APPENDIX A

EFFECT OF HEAT ADDITION ON TOTAL PRESSURE

The main effect of moisture condensation on the details of fluid flow, in particular the effect on the pressure drop, is caused by the release of the heat of vaporization of the condensed water in the fluid. In the following discussion, the effects of condensation are therefore considered as the effect of the addition of heat to a moving gas stream.

When heat is added to a stream of gas moving at a subsonic velocity, a pressure drop occurs in the direction of flow because the velocity of the gas is increased. In ducts of constant cross-sectional area, the change in static pressure is equal but opposite in sign to the change in momentum per unit of area. When the amount of heat added is small and the initial Mach number is small enough that the effect of change in static pressure on density may be neglected, the drop in static pressure between the points 1 and 2 is given by the equation

$$p_1 - p_2 = \rho_1 u_1^2 \frac{t_2 - t_1}{t_1} = \rho_1 u_1^2 \frac{\Delta t}{t_1} \tag{6}$$

The dynamic pressure $\frac{1}{2} \rho u^2$ increases, because of the higher velocity, by the amount $\frac{1}{2} \rho_1 u_1^2 \frac{\Delta t}{t_1}$ and the decrease in the total pressure, H_1 and H_2, is given by the equation

$$H_1 - H_2 = \frac{1}{2} \rho_1 u_1^2 \frac{\Delta t}{t_1} \tag{7}$$

When heat is added to a moving gas stream, a loss of total pressure thus occurs. A correction for this loss in total pressure is automatically introduced by equation (3) when the velocity u_m is the true velocity as determined by a momentum-integrating device such as a thrust target. The correction is exact only for low Mach numbers and only if the hood-discharge velocity is nearly equal to the velocity in the section of the hood in which the heat addition occurs.

The true total pressure $p_2 + \frac{1}{2} \rho_2 u_2{}^2$ is lower than the total pressure before the addition of heat. In equation (1), however, the temperature used, in effect, to calculate the density ρ_2 is not t_2 but t_1. The apparent total pressure H_{2c} at section 2 is therefore

$$H_{2c} = p_2 + \frac{1}{2} \frac{p_2 u_2{}^2}{gRt_1} = p_1 - \rho_1 u_1{}^2 \frac{\Delta t}{t_1} + \frac{1}{2} \frac{p_2 u_2{}^2}{gRt_1} \qquad (8)$$

If the change in pressure is assumed to have a negligible effect in changing the density,

$$H_{2c} = p_2 + \frac{1}{2} \frac{p_2 u_2{}^2}{gRt_2} \frac{t_2}{t_1}$$

$$= p_2 + \frac{1}{2} \frac{p_2 u_2{}^2}{gRt_2} + \frac{1}{2} \frac{p_2 u_2{}^2}{gRt_2} \frac{\Delta t}{t_1}$$

$$= H_2 + \frac{1}{2} \rho_2 u_2{}^2 \frac{\Delta t}{t_1} \qquad (9)$$

The change in Δt has been assumed to be small; hence, the velocity u_2 is nearly equal to the velocity u_1 and
$\frac{1}{2} \rho_2 u_2{}^2 \frac{\Delta t}{t_1} \approx \frac{1}{2} \rho_1 v_1{}^2 \frac{\Delta t}{t_1}$.

The calculated total pressure is therefore equal to the initial total pressure before the addition of heat

$$H_{2c} = H_2 + \frac{1}{2} \rho_1 u_1{}^2 \frac{\Delta t}{t_1} = H_1 \qquad (10)$$

The range of validity of this approximation was investigated by calculating the ratio of H_{2c}/H_1 for a constant-area duct using the equations for compressible flow. The ratio H_{2c}/H_1 was found to be within 1 percent of unity if the product of

$$\left(u_1/\sqrt{gRT_1}\right)^{1.3} \left(\frac{\Delta t}{T_1}\right) < 0.0885 \quad \text{and} \quad u_1/\sqrt{gRT_1} < 1.08, \quad \text{that is, less}$$

than the local velocity of sound.

APPENDIX B

CALCULATION OF THE TOTAL PRESSURE OF A GAS FLOWING IN A TUBE

When the assumption is made that the velocity, the temperature, and the static pressure of a gas flowing through a uniform tube at high Reynolds number are uniform, the total pressure may be calculated from a consideration of the continuity and energy equations and the temperature-pressure relation for an isentropic expansion.

These relations are expressed by the following equations:

$$M = \rho_2 \, u_2 \, A_2 \tag{11}$$

$$t_2 = T_2 - \frac{u_2^2}{\frac{2\gamma}{\gamma - 1} gR} \tag{12}$$

$$\rho_2 = \frac{p_2}{gRt_2} \tag{13}$$

and

$$\left(\frac{H_2}{p_2}\right)^{\frac{\gamma-1}{\gamma}} = \frac{T_2}{t_2} \tag{14}$$

The density term is eliminated by substituting equation (13) in equation (11)

$$\frac{p_2 \, A_2}{M} \, u_2 = gRt_2 \tag{15}$$

and, by use of equations (12) and (15)

$$\frac{2\gamma}{\gamma - 1} \frac{p_2 \, A_2}{M} \, u_2 = \frac{2\gamma}{\gamma - 1} \, gRT_2 - u_2^2. \tag{16}$$

Equation (16) may be solved directly for u_2

$$u_2 = \sqrt{\left(\frac{\gamma}{\gamma - 1} \frac{p_2\,A_2}{M}\right)^2 + \frac{2\gamma}{\gamma - 1}\,gRT_2} - \left(\frac{\gamma}{\gamma - 1}\frac{p_2\,A_2}{M}\right) \qquad (17)$$

The combination of equations (12), (14), and (17) gives the relation

$$\left(\frac{H_2}{p_2}\right)^{\frac{\gamma - 1}{\gamma}} = \frac{\dfrac{2\gamma}{\gamma - 1}\,gRT_2}{\dfrac{2\gamma}{\gamma - 1}\,gRT_2 - u_2^{\,2}}$$

$$= \frac{\dfrac{2\gamma}{\gamma - 1}\,gRT_2}{2\,\dfrac{\gamma}{\gamma - 1}\dfrac{p_2\,A_2}{M}\left[\sqrt{\left(\dfrac{\gamma}{\gamma-1}\dfrac{p_2\,A_2}{M}\right)^2 + \dfrac{2\gamma}{\gamma-1}\,gRT_2} - \left(\dfrac{\gamma}{\gamma-1}\dfrac{p_2\,A_2}{M}\right)\right]}$$

$$(18)$$

When the radical is removed from the denominator of equation (18), the relation for the ratio of total pressure to static pressure becomes

$$\left(\frac{H_2}{p_2}\right)^{\frac{\gamma - 1}{\gamma}} = \left[\frac{\sqrt{\left(\dfrac{\gamma}{\gamma - 1}\dfrac{p_2\,A_2}{M}\right)^2 + \dfrac{2\gamma}{\gamma - 1}\,gRT_2}}{2\left(\dfrac{\gamma}{\gamma - 1}\dfrac{p_2\,A_2}{M}\right)} + \frac{1}{2}\right] \qquad (19)$$

In the case of a turbine, where work is abstracted at the wheel, the total temperature of the gas after passing through the wheel T_2 is lower than the temperature of the gas in the nozzle box T_1 by the temperature difference corresponding to the work abstracted at the wheel; that is

$$T_2 = T_1 - \frac{P}{\dfrac{\gamma}{\gamma - 1}\,gRM} \qquad (20)$$

Upon the substitution of equation (20) in equation (19), the following equation for the total pressure is obtained:

$$\frac{H_2}{p_2} = \left[\frac{\sqrt{\left(\frac{\gamma}{\gamma-1} \frac{p_2 A_2}{M}\right)^2 + \frac{2\gamma}{\gamma-1} gRT_1 - 2\frac{P}{M}}}{2\left(\frac{\gamma}{\gamma-1} \frac{p_2 A_2}{M}\right)} + \frac{1}{2} \right]^{\frac{\gamma}{\gamma-1}} \tag{5}$$

When equation (5) is applied to the conditions of the gas discharged from the buckets of a turbine, the effect of any tangential components of velocity is neglected in computing the static gas temperature and also in computing the total useful velocity.

APPENDIX C

CORRECTION OF THE CALCULATED HOOD-DISCHARGE VELOCITY

FOR HUMIDITY OF THE AIR

Because of the high apparent specific heat of the mixture of
air and water just below the dew-point temperature, the temperature
drop in the hood was less when condensation occurred than that cal-
culated for dry air. Calculation shows, however, that the differ-
ence between the mean density of air with a small amount of condensed
water and that of dry air is negligible. Figure 15 was therefore
prepared showing the enthalpy and density of dry air and the enthalpy
of air with various absolute humidities as a function of the tempera-
ture for a pressure of 1 atmosphere.

The correction of the calculated hood-discharge velocity u_c
for effect of condensation was applied by calculating the dry-air
downstream temperature and finding the corresponding density ρ_d
and enthalpy on the chart. The true discharge temperature is found
at the same enthalpy on the line corresponding to the absolute
humidity. The corrected, or wet, density ρ_w is found at this true
temperature. The corrected value of the calculated velocity u_c'
is then given by the equation

$$u_c' = u_c \frac{\rho_d}{\rho_w}$$

The use of figure 15 is shown by the following example:
Determine the correction to the calculated velocity when air with
an absolute humidity of 60 grains per pound and an initial temper-
ature of 80° F is discharged at a pressure of 1 atmosphere after
the removal of 12.5 Btu per pound of air in a turbine. The enthalpy
of the air is 19.2 Btu per pound and its final enthalpy 6.7 Btu per
pound. The dry temperature is 28° F and the wet temperature 42° F.
The corresponding dry and wet densities are 0.0811 and 0.0784 pound
per cubic foot, respectively. The correction factor ρ_d/ρ_w is
equal to 1.035.

APPENDIX D

EVALUATION OF A NOZZLE SURVEY WITH SWIRL ABOUT THE AXIS OF SYMMETRY

The thrust produced by the flow from a nozzle may be obtained by evaluation of the integral

$$F = \iint \rho \, u_a^2 \, dA + \iint (p - p_0) \, dA \tag{21}$$

where

p local static pressure

p_0 atmospheric pressure

u_a axial component of velocity of flow from nozzle

When a survey is made of the flow from a nozzle, the total pressure and the direction of each radial element is measured. If the nozzle is small and the velocity high, measurement of the static pressure is very difficult. When axial symmetry exists in the flow, the radial variation of the static pressure may be estimated, however, from a knowledge of the static pressure on the wall of the nozzle and of the measured values of total pressure and direction of the flow as a function of radius. A radial distribution of total temperature must be measured or assumed.

The radial pressure gradient is given by the differential equation

$$\frac{\partial p}{\partial r} = \rho \, \frac{u_t^2}{r} \tag{22}$$

where

u_t tangential component of velocity of flow from nozzle

The density ρ is given by the equation

$$\rho = \frac{p}{gRt} = \frac{p}{gR\left(T - \dfrac{\gamma - 1}{2\gamma \, gR} \, U^2\right)} \tag{23}$$

where $u_t = U \sin \theta$

and

U   absolute velocity of fluid

θ angle of velocity vector measured from   plane through axis of
       nozzle and point of survey

The differential equation (22) then becomes

$$\frac{1}{p} \frac{\partial p}{\partial r} - \frac{1}{r} \frac{U^2 \sin^2 \theta}{gRT - \frac{\gamma - 1}{\gamma} U^2} = 0 \qquad (24)$$

The velocity U^2 is given by the equation

$$U^2 = \frac{2\gamma}{\gamma - 1} gRT \left[1 - \left(\frac{p}{H}\right)^{\frac{\gamma-1}{\gamma}} \right] \qquad (25)$$

When the value of U^2 from equation (25) is substituted in
equation (24), the following differential equation is obtained

$$\frac{1}{p} \frac{\partial p}{\partial r} = \frac{2\gamma \left[\left(\frac{H}{p}\right)^{\frac{\gamma-1}{\gamma}} - 1 \right] \sin^2 \theta}{(\gamma - 1)r} \qquad (26)$$

Equation (26) cannot be separated into independent variables
because H is a variable, known as a function of r, but it can be
solved when written as an integral equation, by a process of suc-
cessive approximation to determine p as a function of r:

$$\log_e p = \int \frac{2\gamma}{\gamma - 1} \left[\left(\frac{H}{p}\right)^{\frac{\gamma-1}{\gamma}} - 1 \right] \sin^2 \theta \frac{dr}{r} \qquad (27)$$

This integration process converges rapidly except at the center of
the nozzle where it may not converge to a physically significant

pressure. It is necessary to assume that the flow becomes a "solid-body" flow near the center; that is, the tangential velocity is proportional to the radius. A new form of the integral equation is more convenient for this central core, namely

$$\log_e p = \int \frac{u_t^2 \, dr}{r \left(gRT - \frac{\gamma - 1}{2\gamma} u_t^2 \csc^2 \theta \right)} \tag{28}$$

The value of θ in this central core may be obtained with sufficient accuracy either by extrapolation of values of θ measured outside this core or by assuming that $\tan \theta$ equals u_t/u_a, where u_a is assumed constant. This assumption is valid only in the region very near $r = 0$. The axial velocity u_a will be negative near the axis when a flow reversal occurs.

The mass flow may be obtained from the static-pressure distribution calculated with the aid of equations (27) and (28) by the use of the following equation:

$$M = \iint \rho u_a \, dA = \int \sqrt{\frac{2\gamma}{(\gamma-1)gRT} \left(\frac{H}{p}\right)^{\frac{\gamma-1}{\gamma}} \left[\left(\frac{H}{p}\right)^{\frac{\gamma-1}{\gamma}} - 1 \right]} \; p \cos \theta \; 2\pi r dr \tag{29}$$

REFERENCE

1. Pinkel, Benjamin, Turner, L. Richard, and Voss, Fred: Design of Nozzles for the Individual Cylinder Exhaust Jet-Propulsion System. NACA ACR, April 1941.
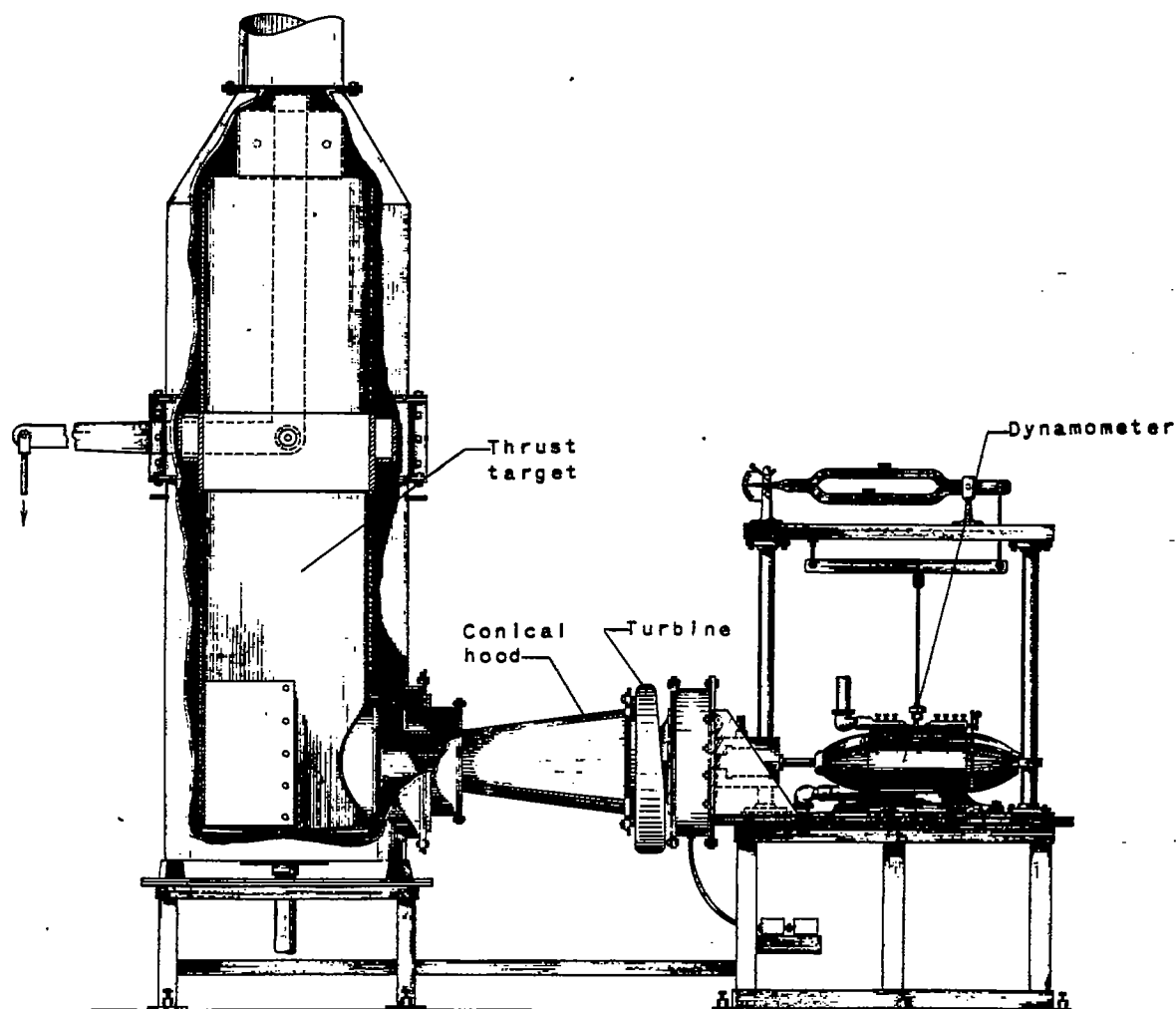
Figure 1. – Setup for turbine-hood performance tests.

Fig. 2
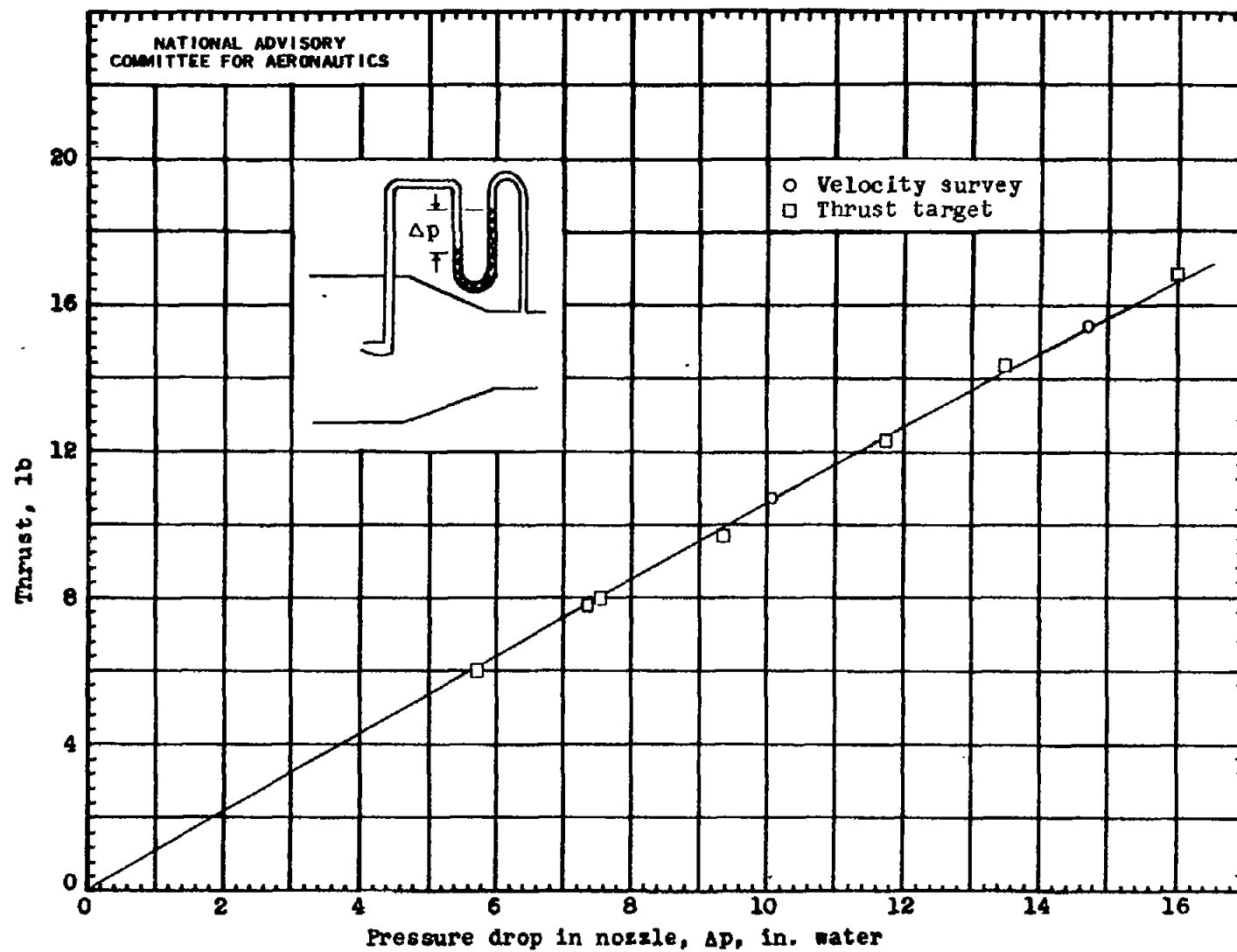
Figure 2. — Calibration of thrust target.
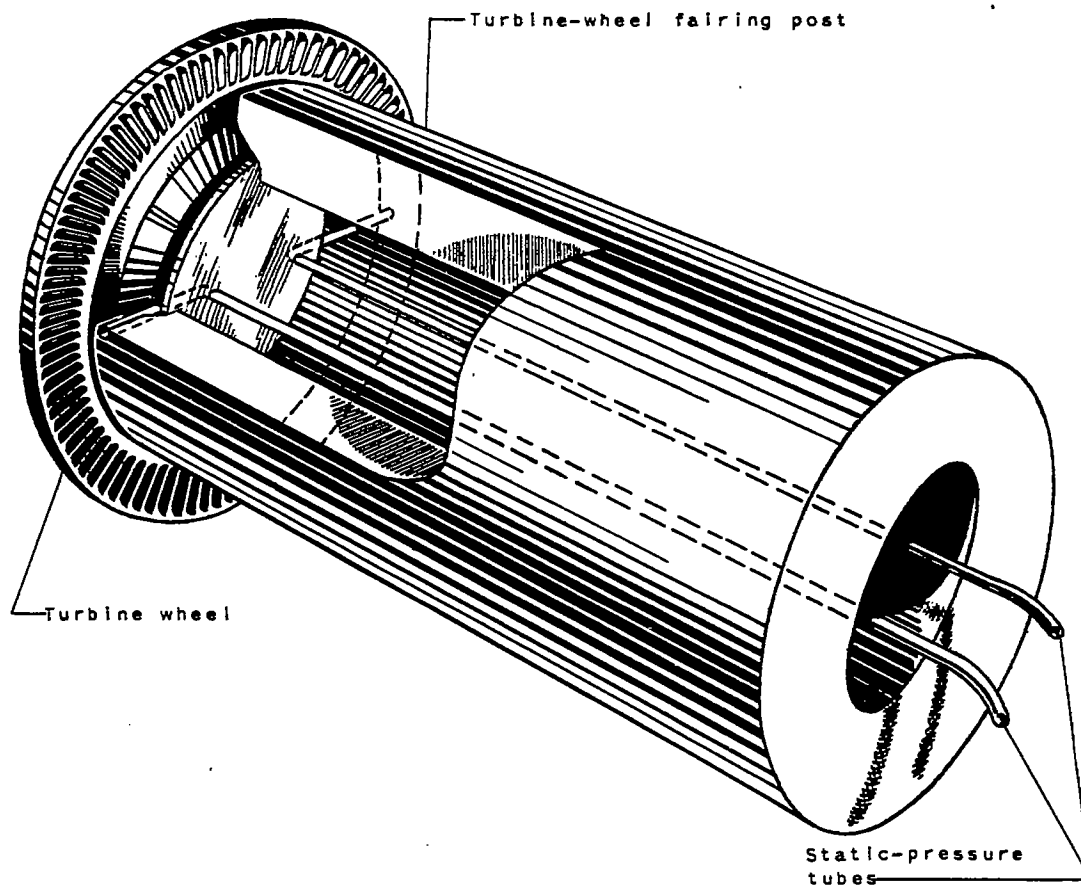
Turbine-wheel fairing post

Turbine wheel

Static-pressure tubes

(a)   Sketch of turbine wheel and fairing post.

Figure 3. – Turbine calibration.
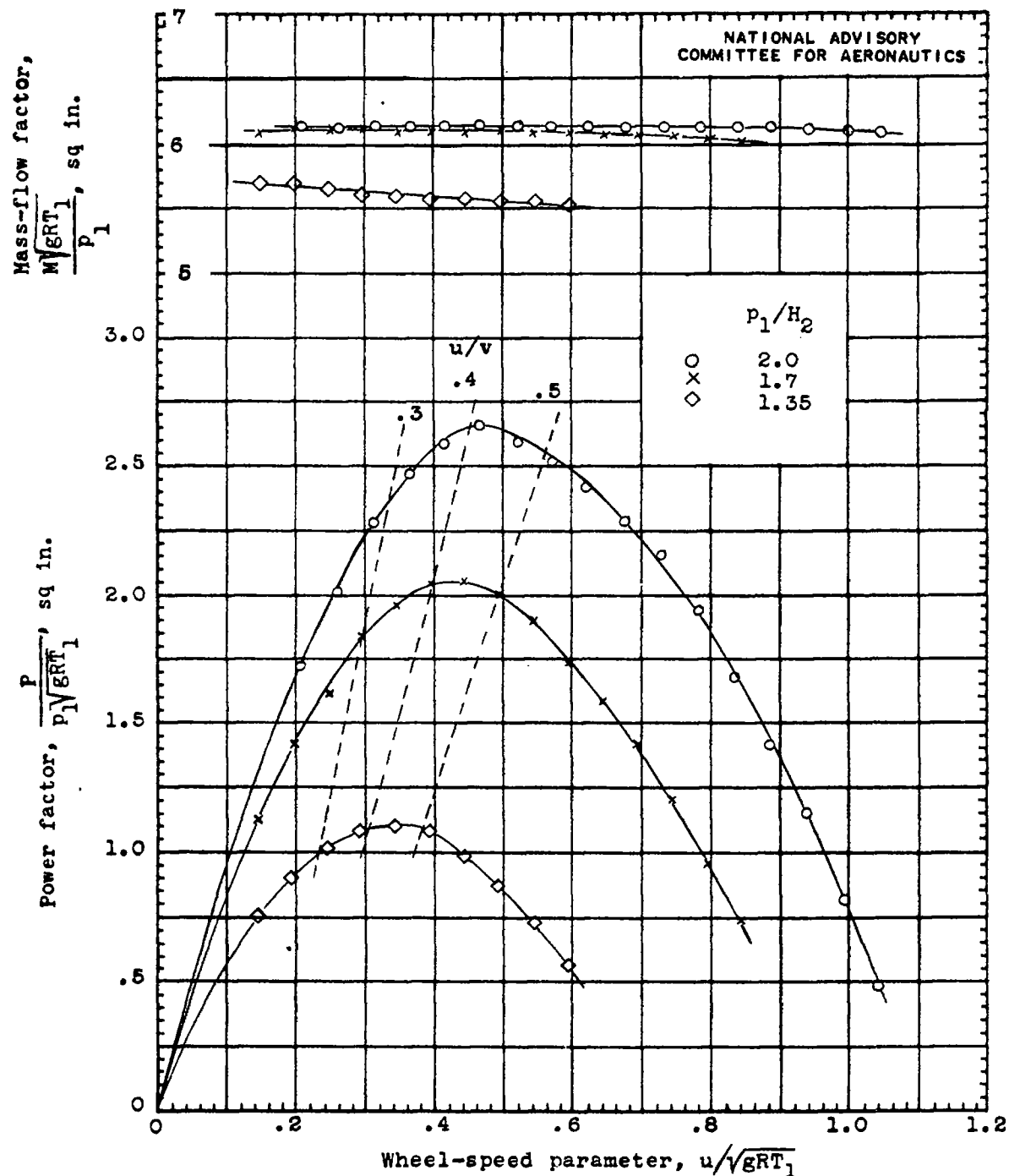
(b) Variation of power and mass flow with wheel-speed
parameter for turbine calibration.

Figure 3. – Concluded. Turbine calibration.

NACA TN No. 1149
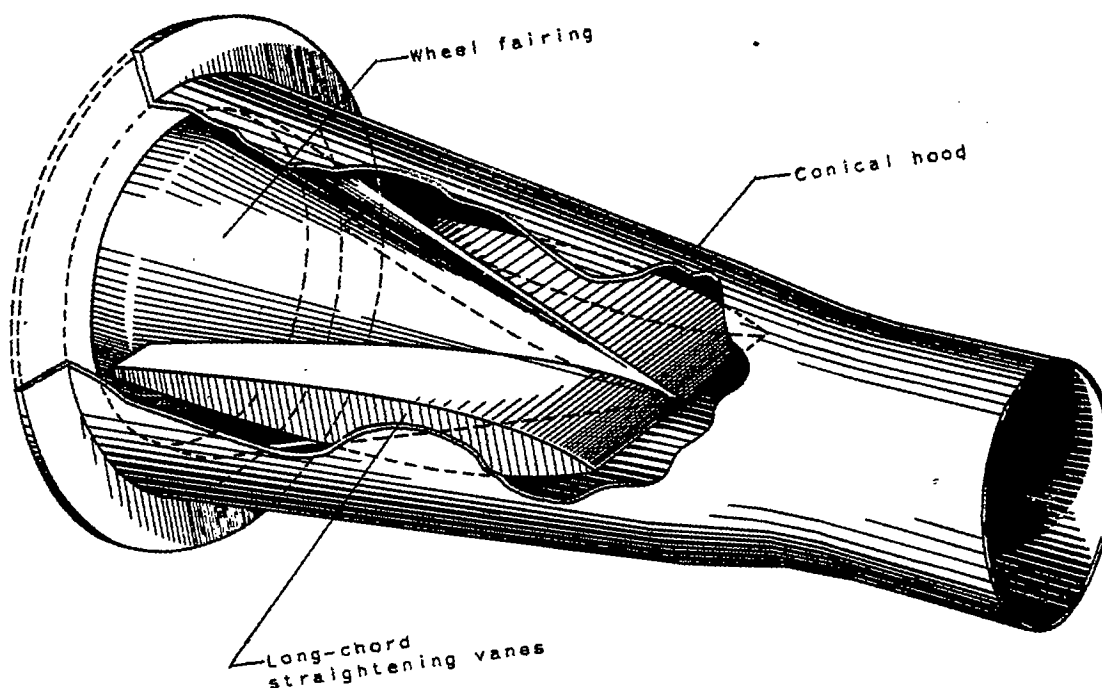
(a) Sketch of hood.

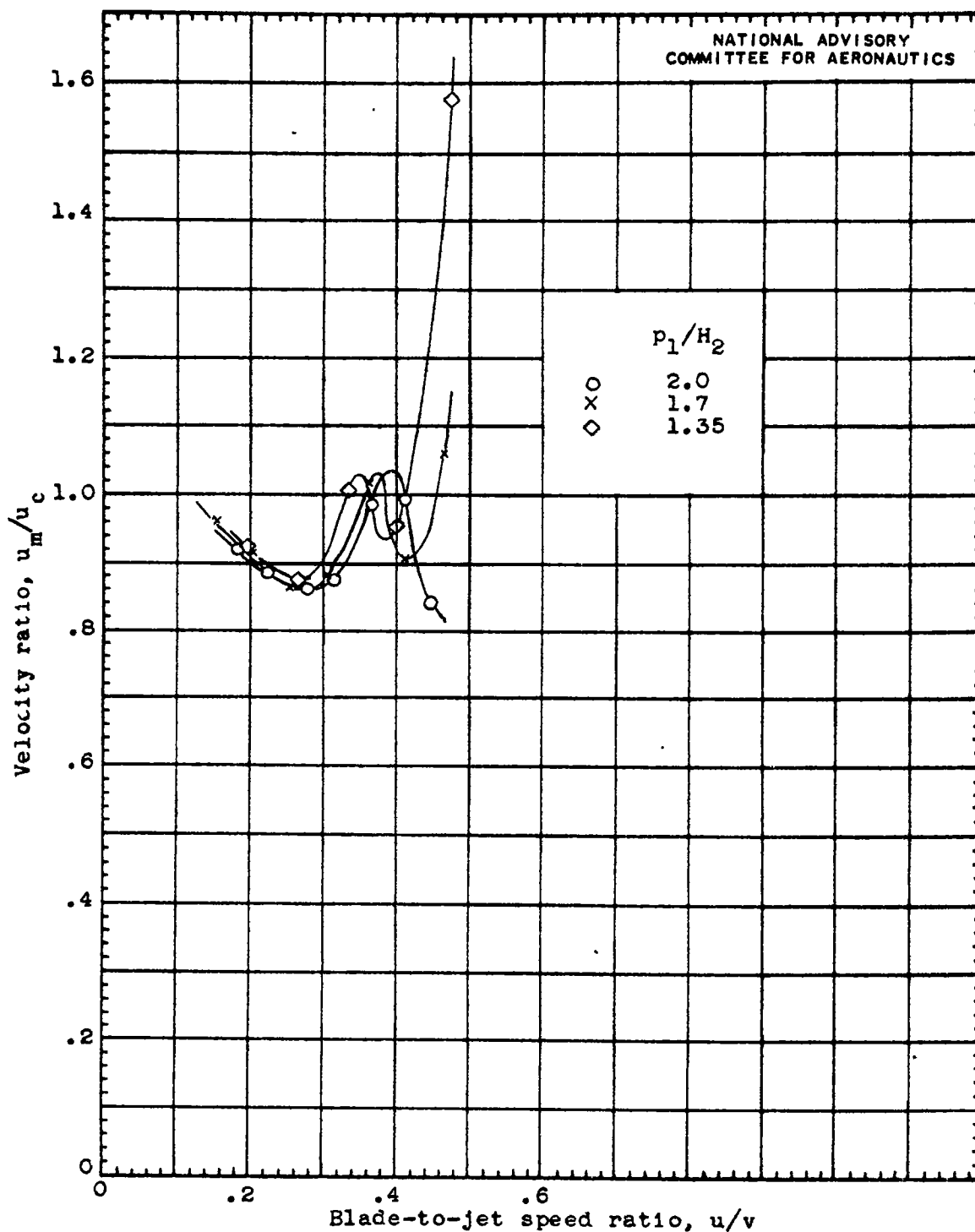Figure 4. – Conical hood with long-chord straightening vanes and wheel fairing.
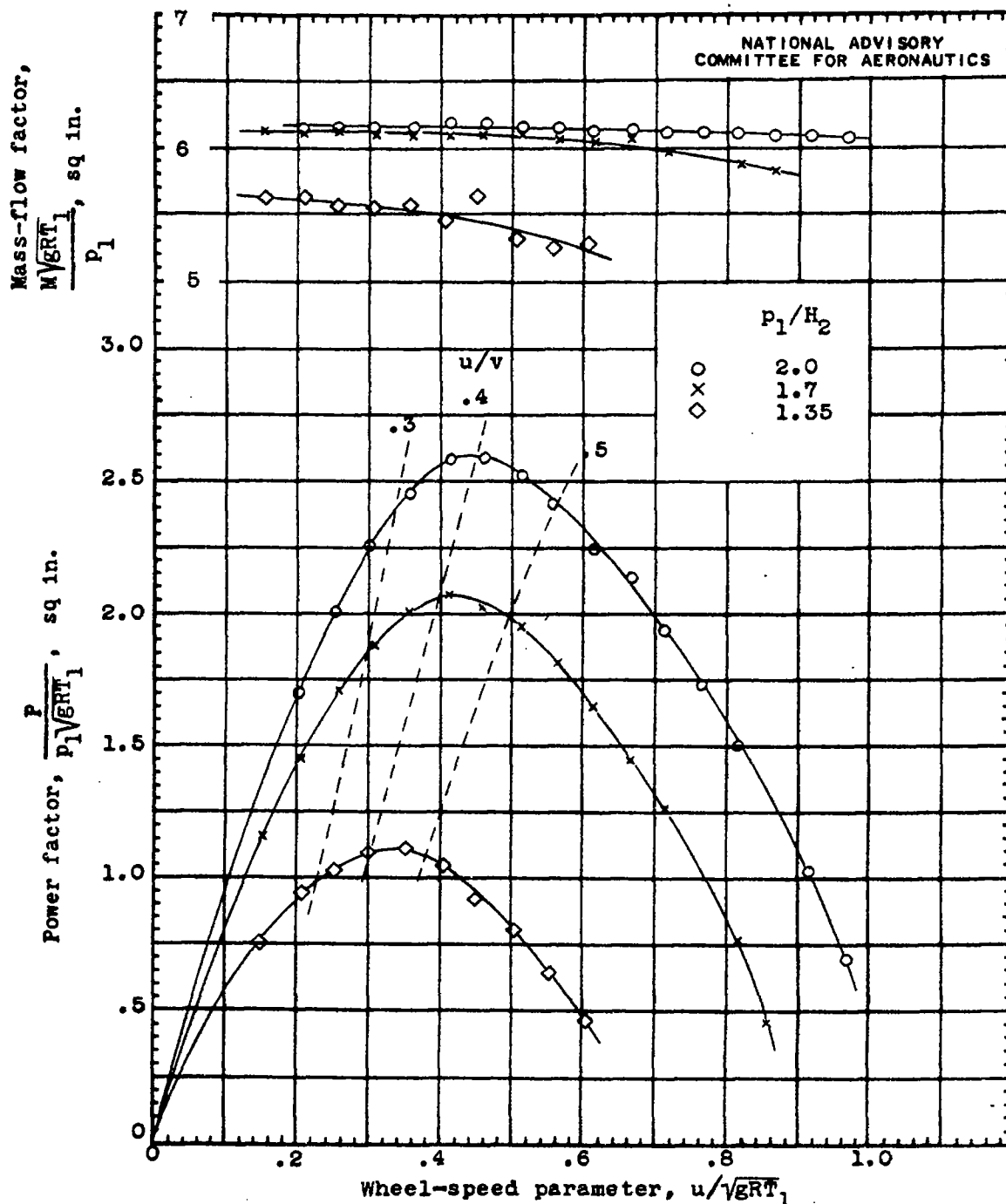
(b) Variation of power and mass flow of turbine-hood
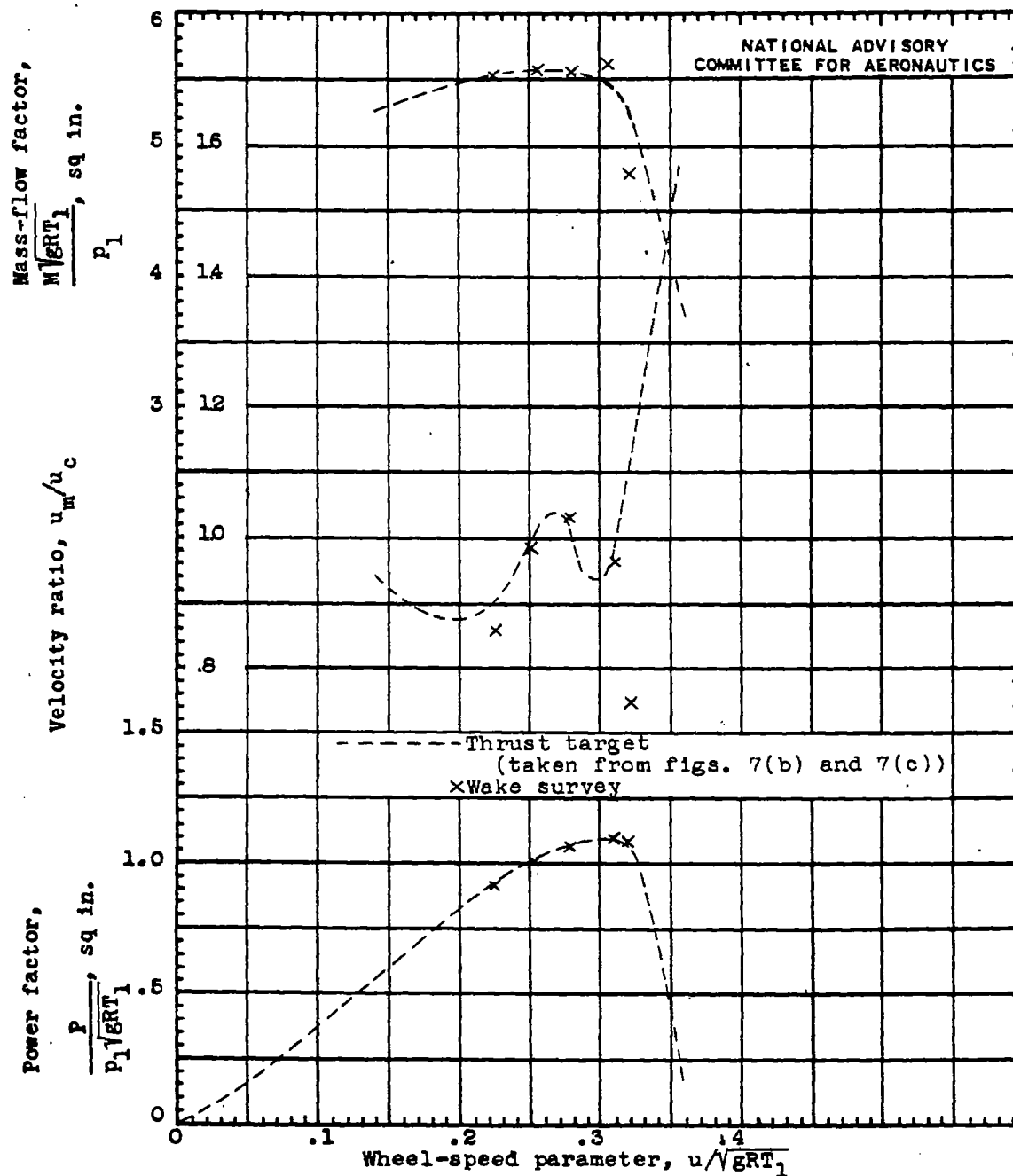combination with wheel-speed parameter.

Figure 4. - Continued.   Conical hood with long-chord straighten-
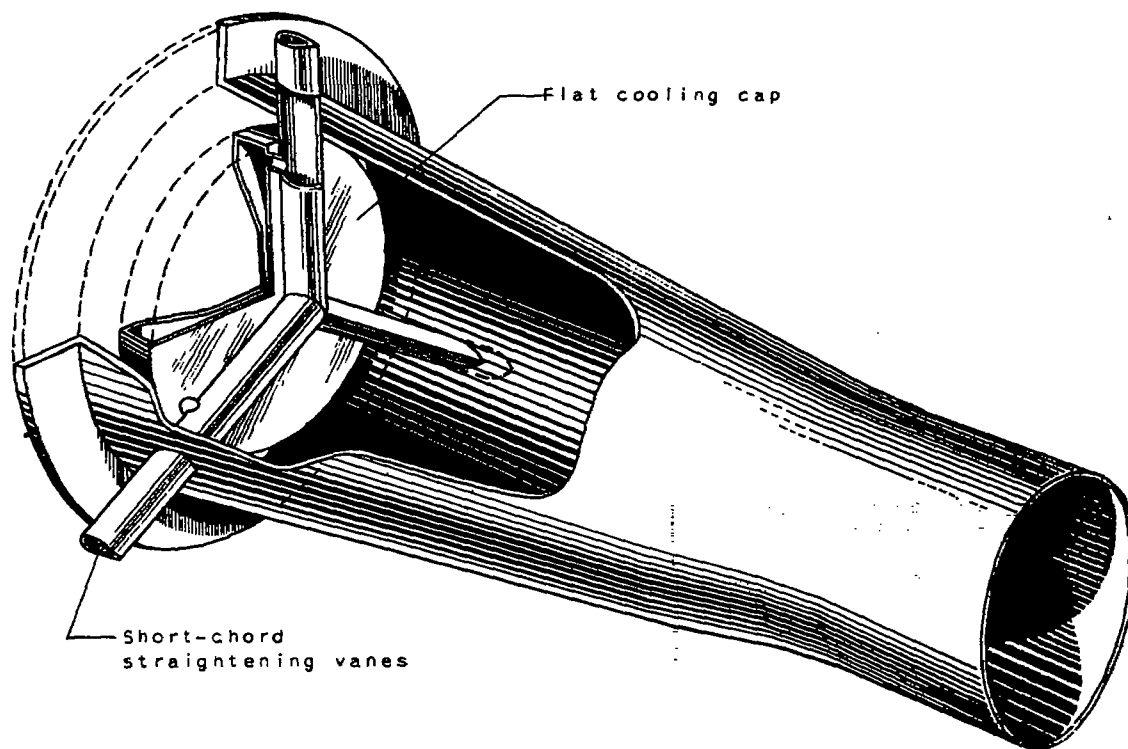ing vanes and wheel fairing.
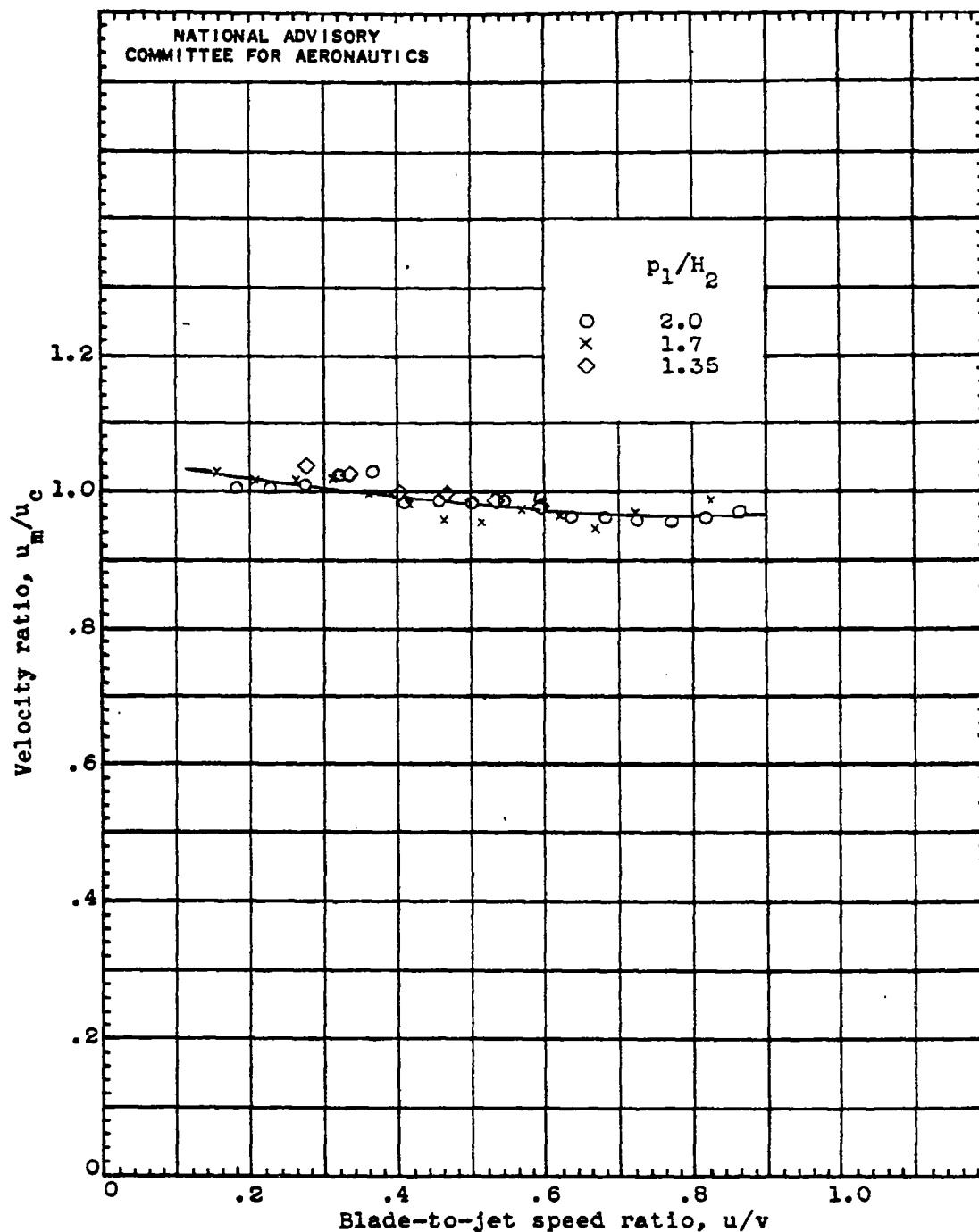
(c) Variation of ratio of effective hood-discharge
velocity to calculated hood-discharge velocity
u_m/u_c with blade-to-jet speed ratio.

Figure 4. - Concluded.   Conical hood with long-chord straightening
vanes and wheel fairing.

Entrance fairing band

Turbine buckets
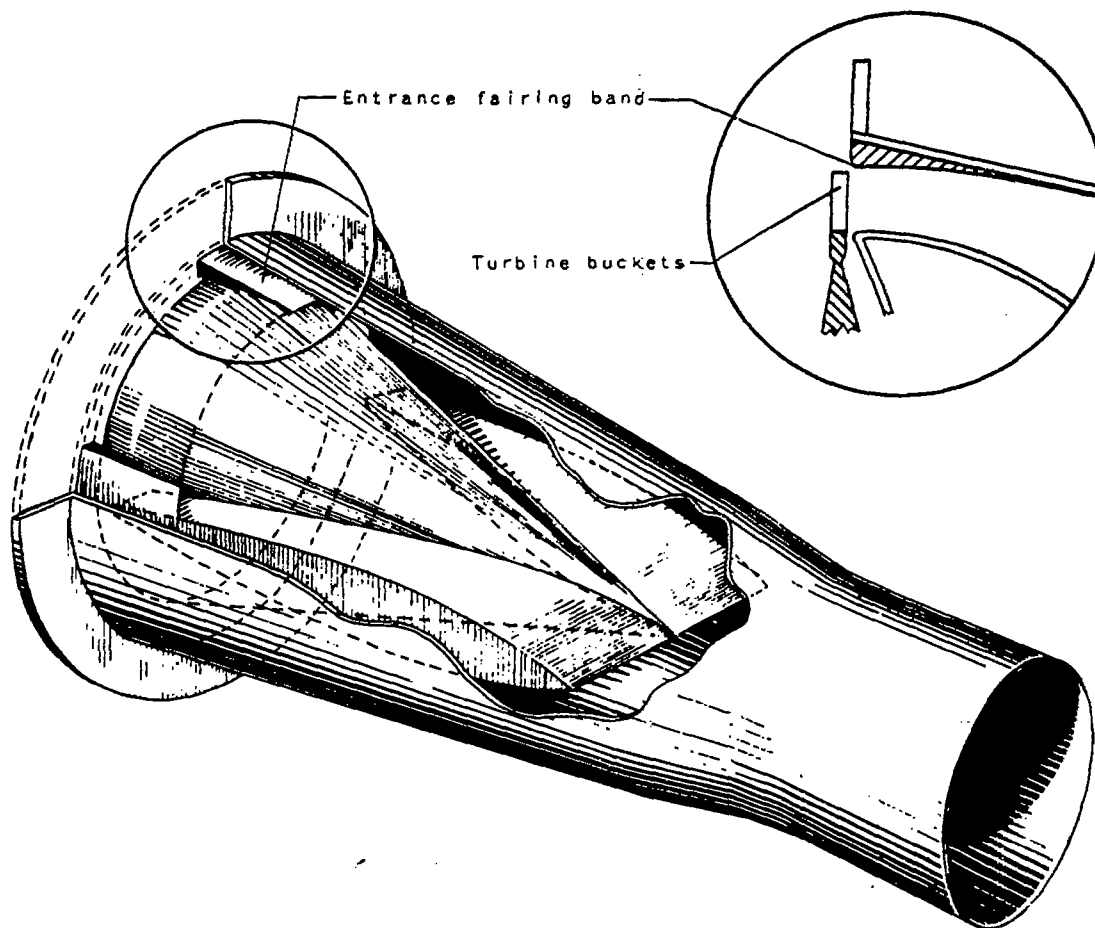
(a)   Sketch of hood.

Figure 5. - Conical hood with long-chord straightening vanes,
wheel fairing, and hood-entrance fairing band.

166-285

NATIONAL ADVISORY
COMMITTEE FOR AERONAUTICS
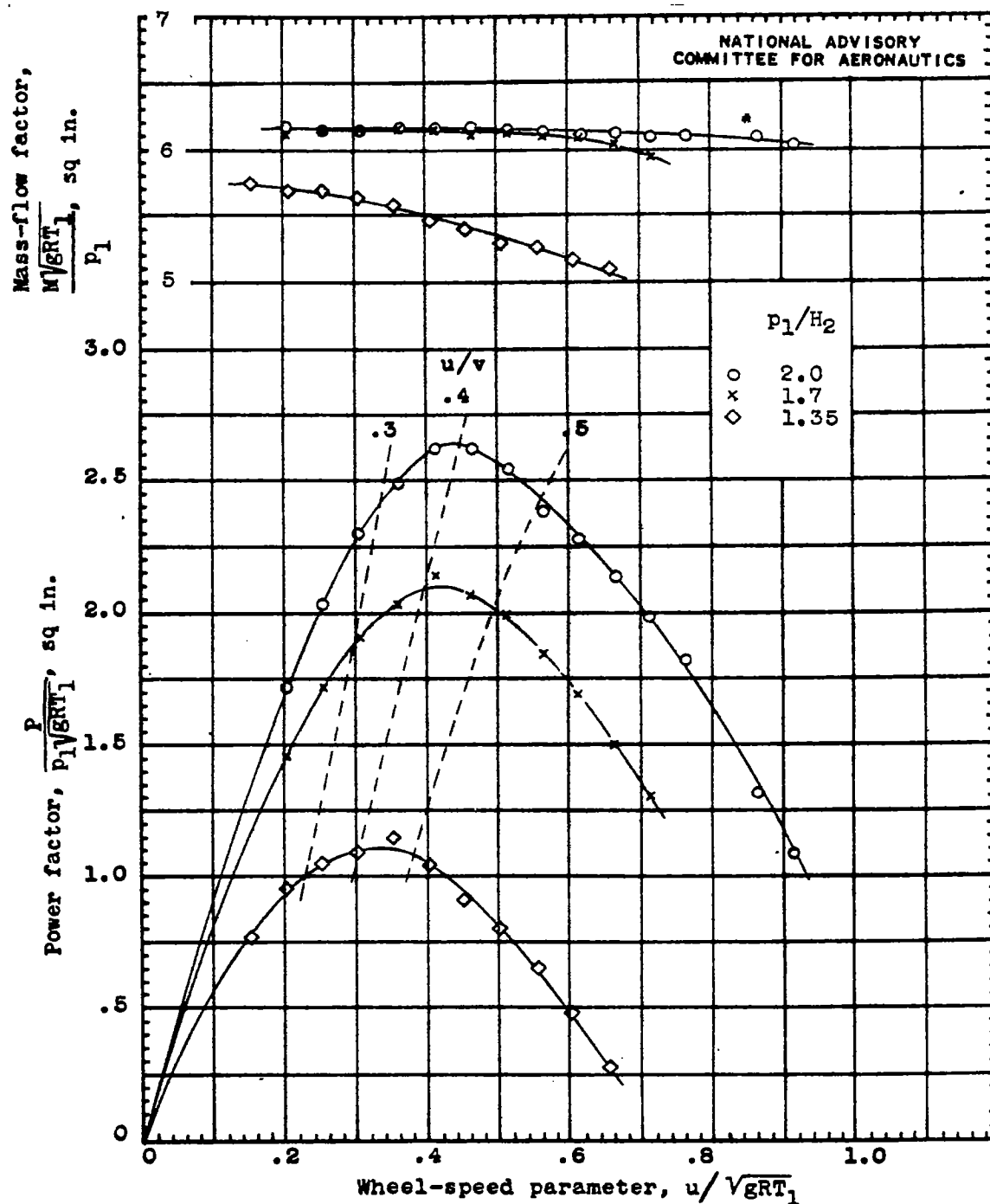
(b) Variation of power and mass flow of turbine-hood
combination with wheel-speed parameter.

Figure 5. — Continued. Conical hood with long-chord straighten-
ing vanes, wheel fairing, and hood-entrance fairing band.
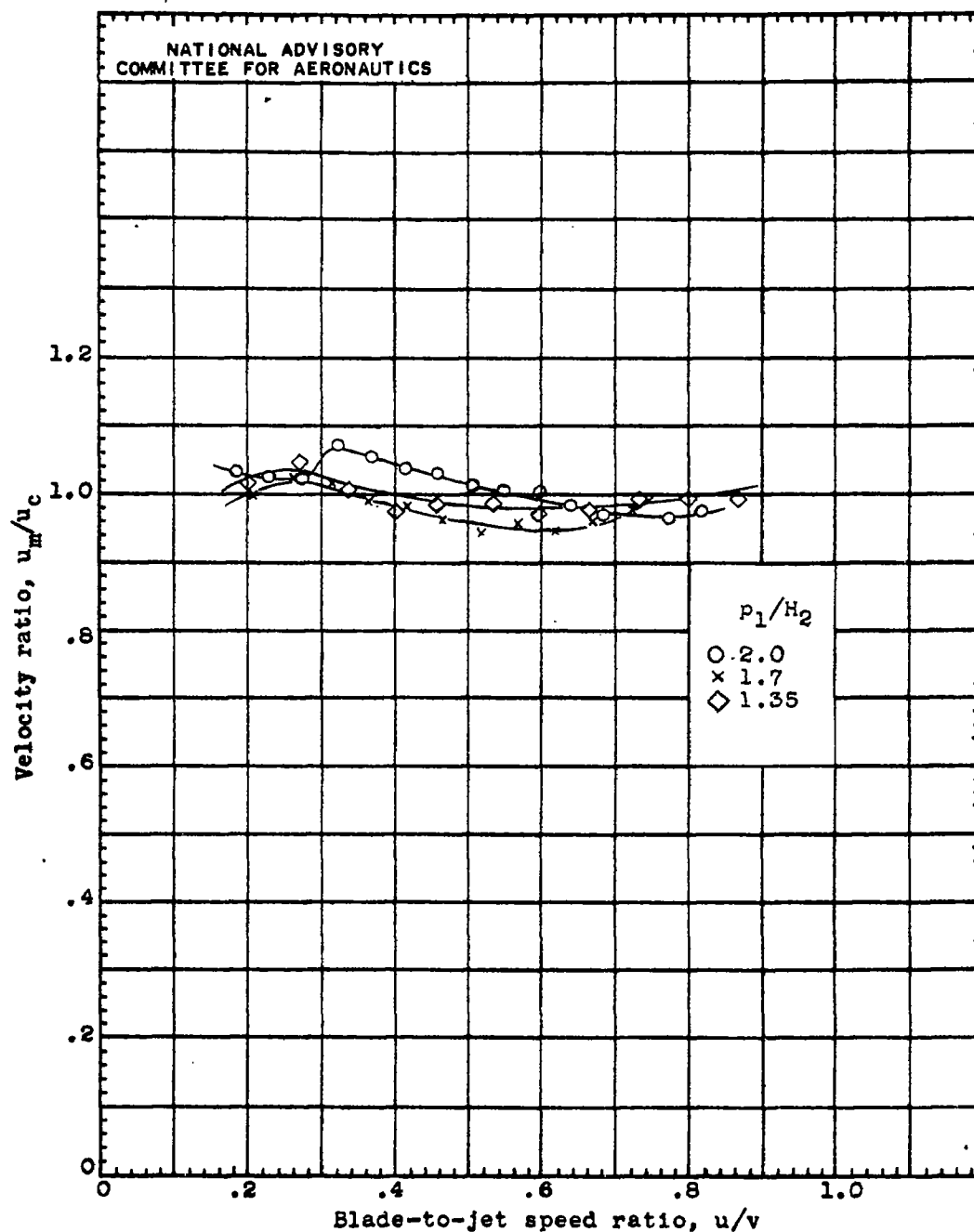
(c) Variation of the ratio of effective hood-discharge
    velocity to calculated hood-discharge velocity
    u_m/u_c with blade-to-jet speed ratio.

Figure 5. - Concluded. Conical hood with long-chord straightening
    vanes, wheel fairing, and hood-entrance fairing band.
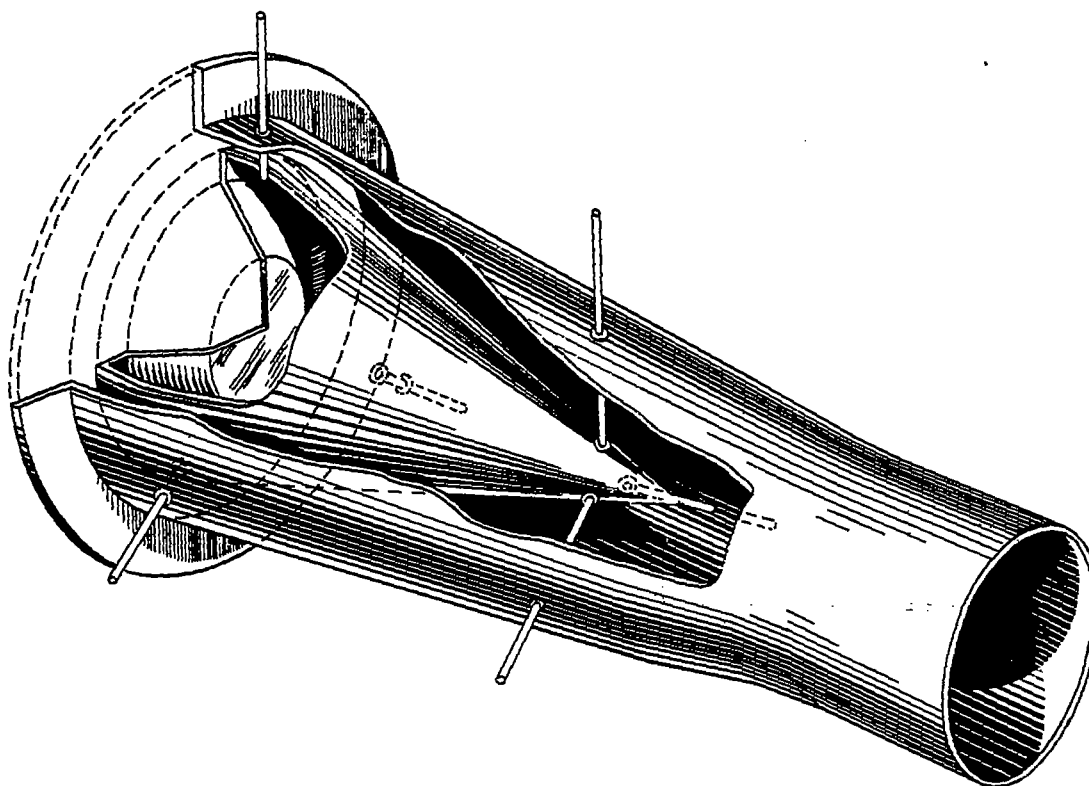
**NATIONAL ADVISORY
COMMITTEE FOR AERONAUTICS**

(a) Sketch of hood.

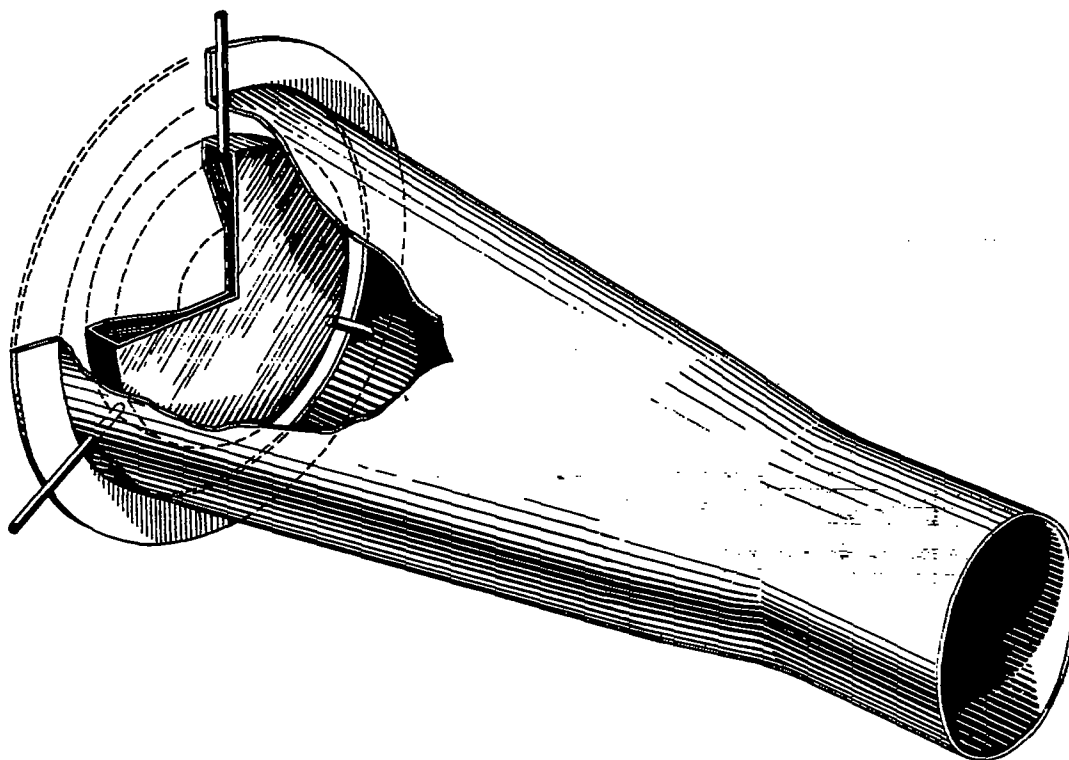Figure 6. - Conical hood with wheel fairing supported by $\frac{3}{8}$-inch tubes.
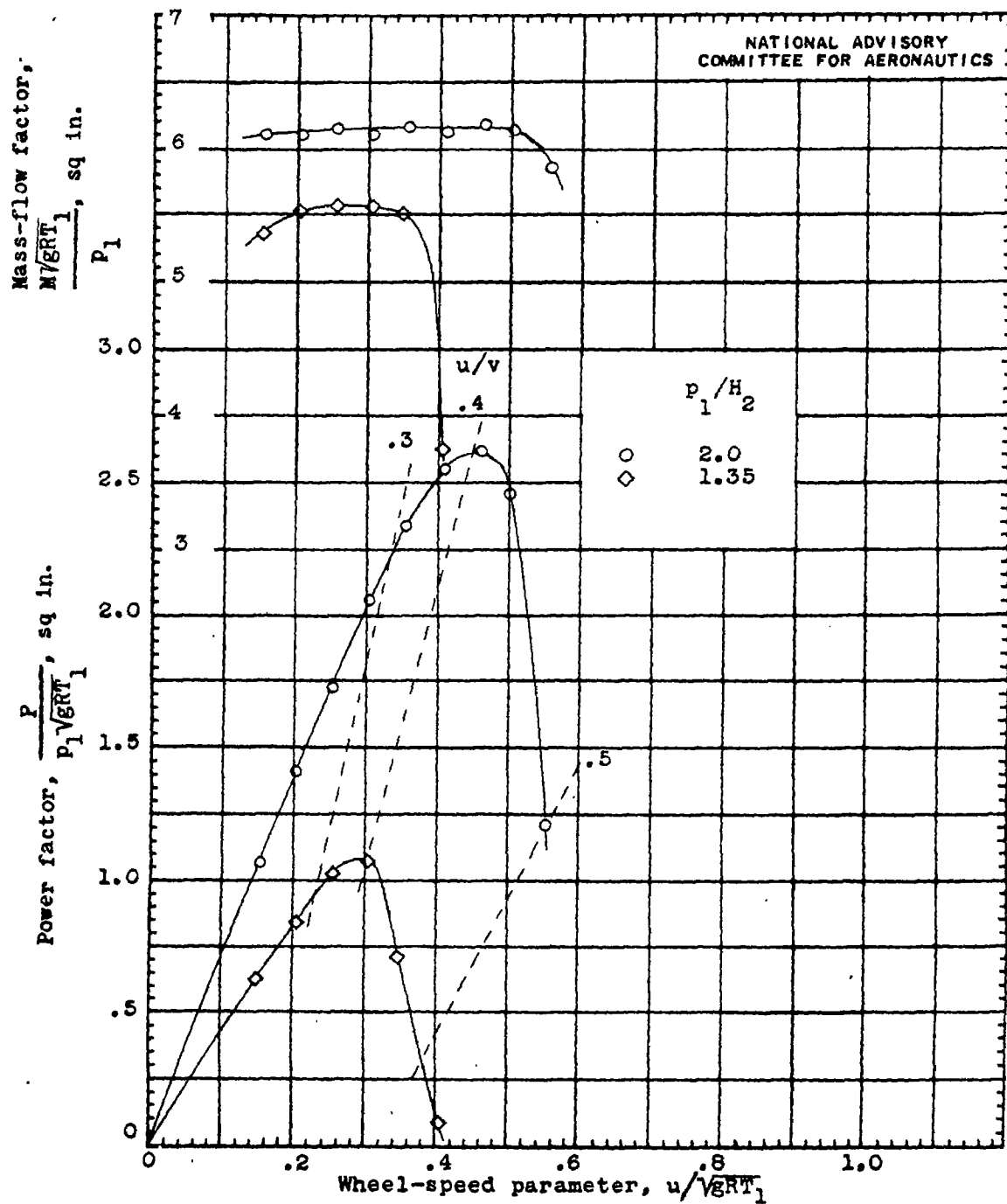
(b) Variation of power and mass flow of turbine-hood
combination with wheel-speed parameter.

Figure 6. - Continued.   Conical hood with wheel fairing
supported by 3/8-inch tubes.
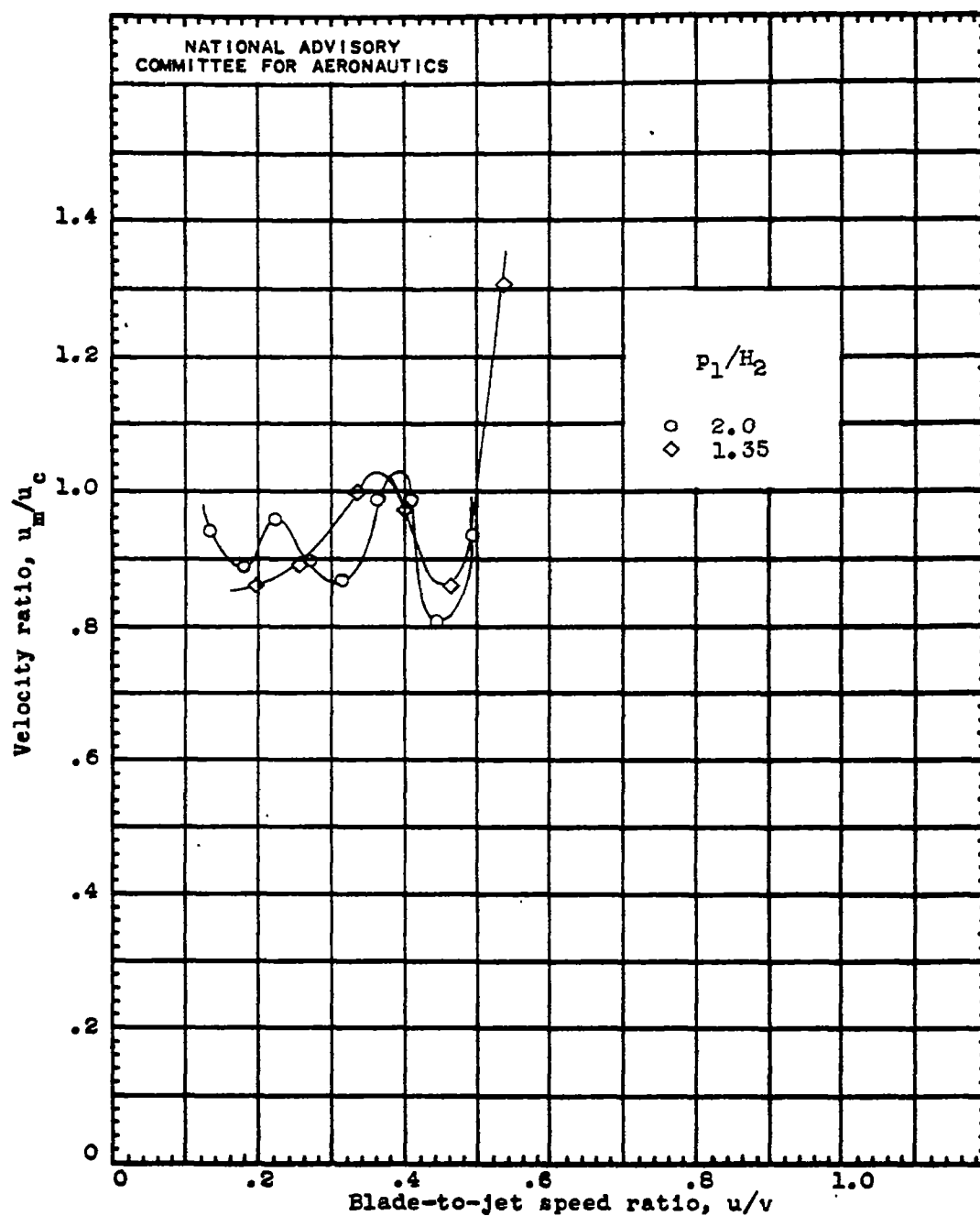
(c) Variation of ratio of effective hood-discharge
velocity to calculated hood-discharge velocity
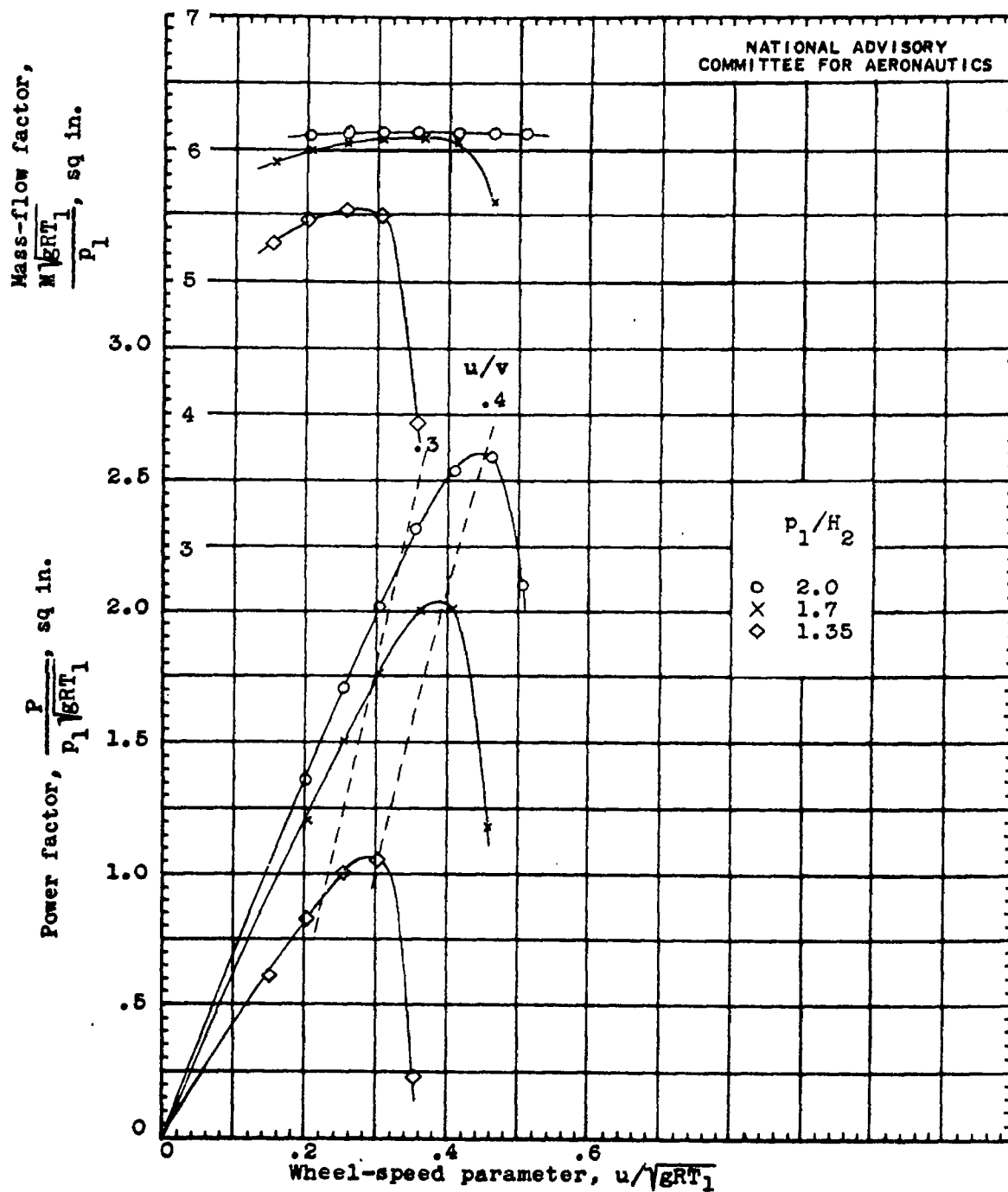u_m/u_c with blade-to-jet speed ratio.

Figure 6. – Concluded. Conical hood with wheel fairing supported
by 3/8-inch tubes.

NATIONAL ADVISORY
COMMITTEE FOR AERONAUTICS
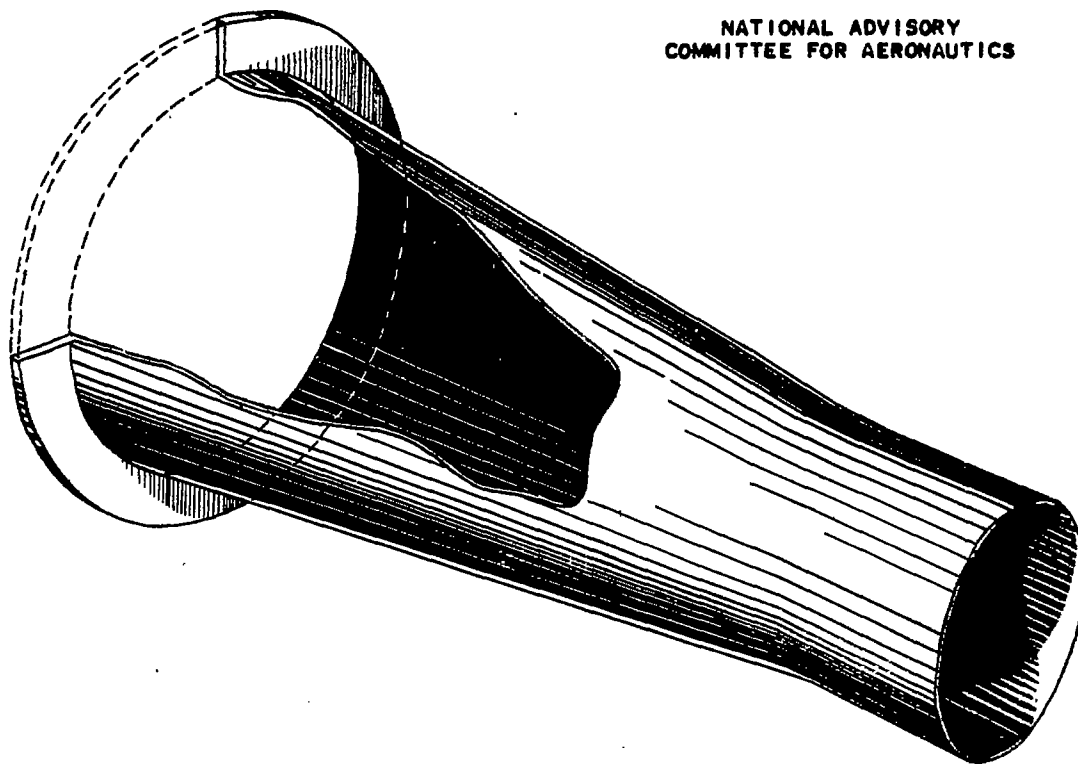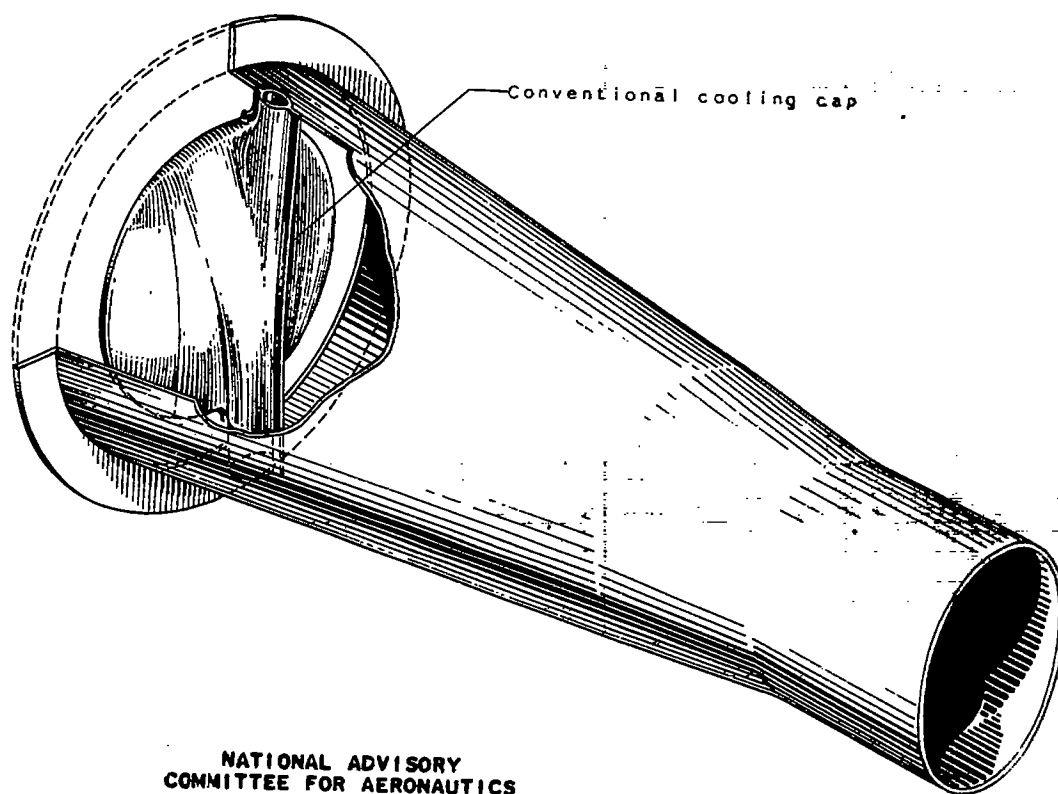
(a) Sketch of hood.

Figure 7. – Plain conical hood.
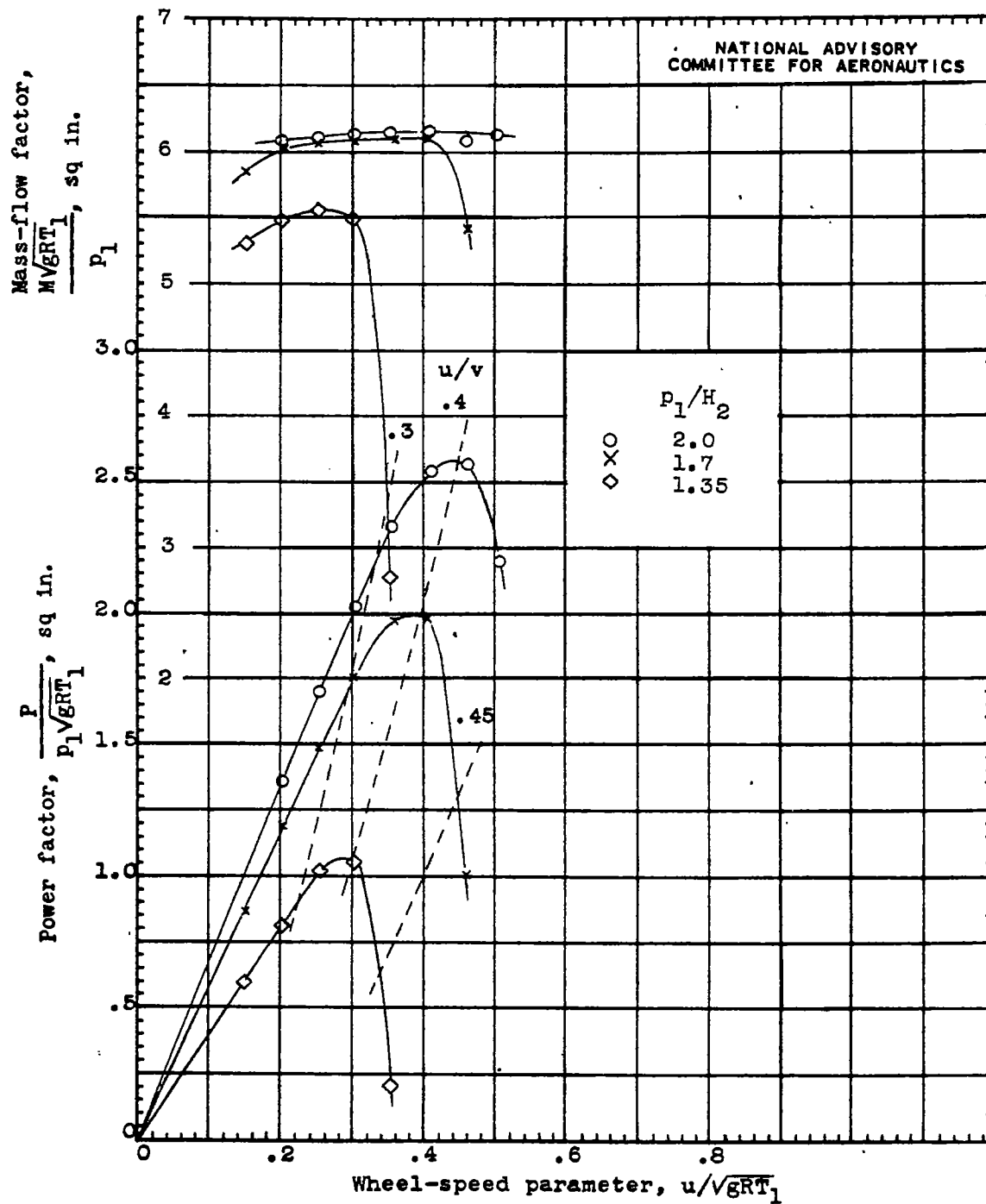
(b) Variation of power and mass flow of turbine-hood
combination with wheel-speed parameter .

Figure 7. — Continued.   Plain conical hood.

(c) Variation of the ratio of effective hood-discharge
    velocity to calculated hood-discharge velocity
    u_m/u_c with blade-to-jet speed ratio.

Figure 7. — Continued.   Plain conical hood.

(d) Comparison of performance characteristics of turbine and
conical hood as determined by thrust target and by
survey of jet discharged from hood. Pressure ratio,
p_1/H_2, 1.35.

Figure 7. — Concluded. Plain conical hood.

Flat cooling cap

Short-chord
straightening vanes

NATIONAL ADVISORY
COMMITTEE FOR AERONAUTICS

(a)   Sketch of hood.

Figure 8. - Conical hood with flat cooling cap and short-
   chord straightening vanes.
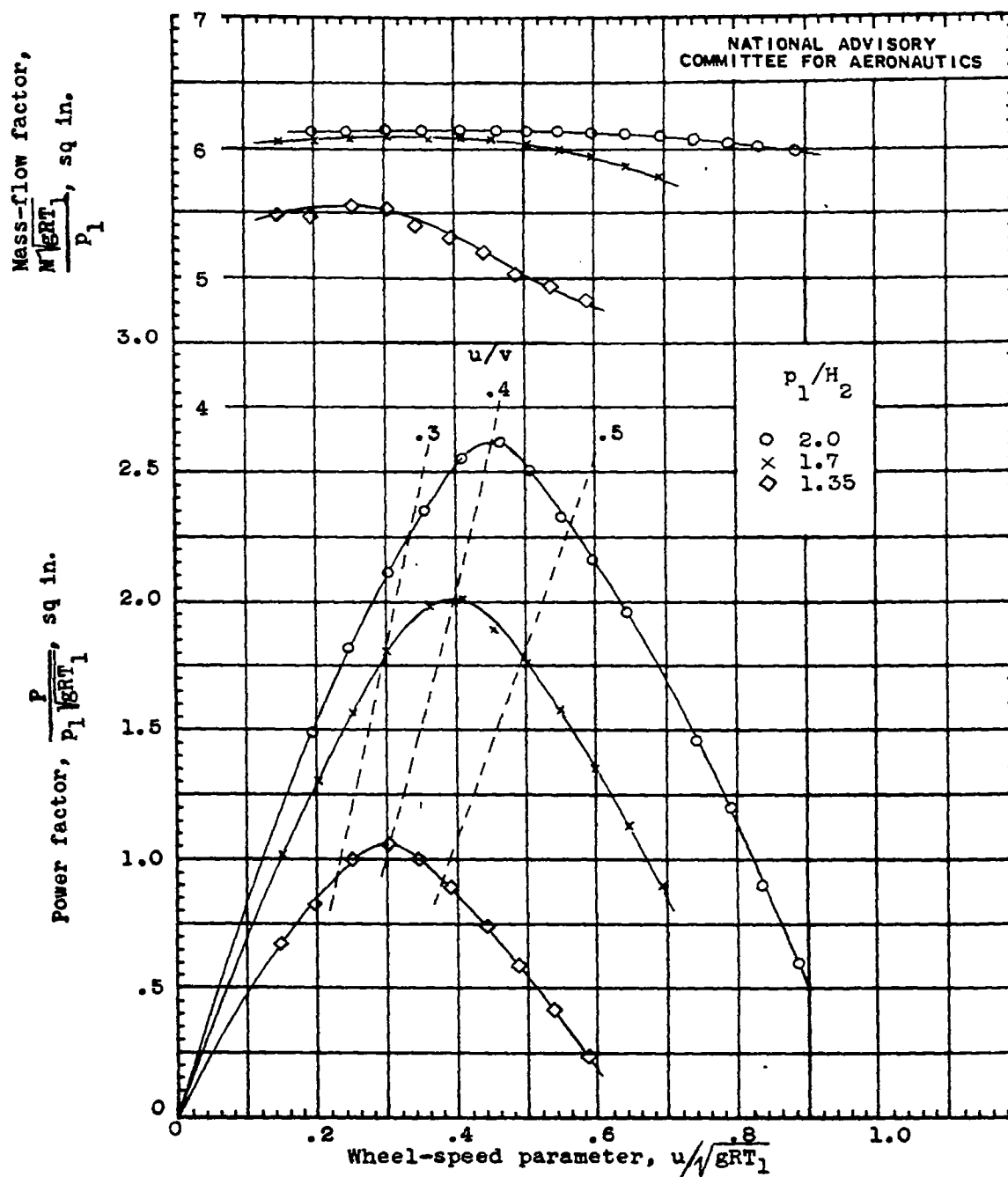
(b) Variation of power and mass flow of turbine-hood
combination with wheel-speed parameter.

Figure 8. – Continued. Conical hood with flat cooling cap and
short-chord straightening vanes.
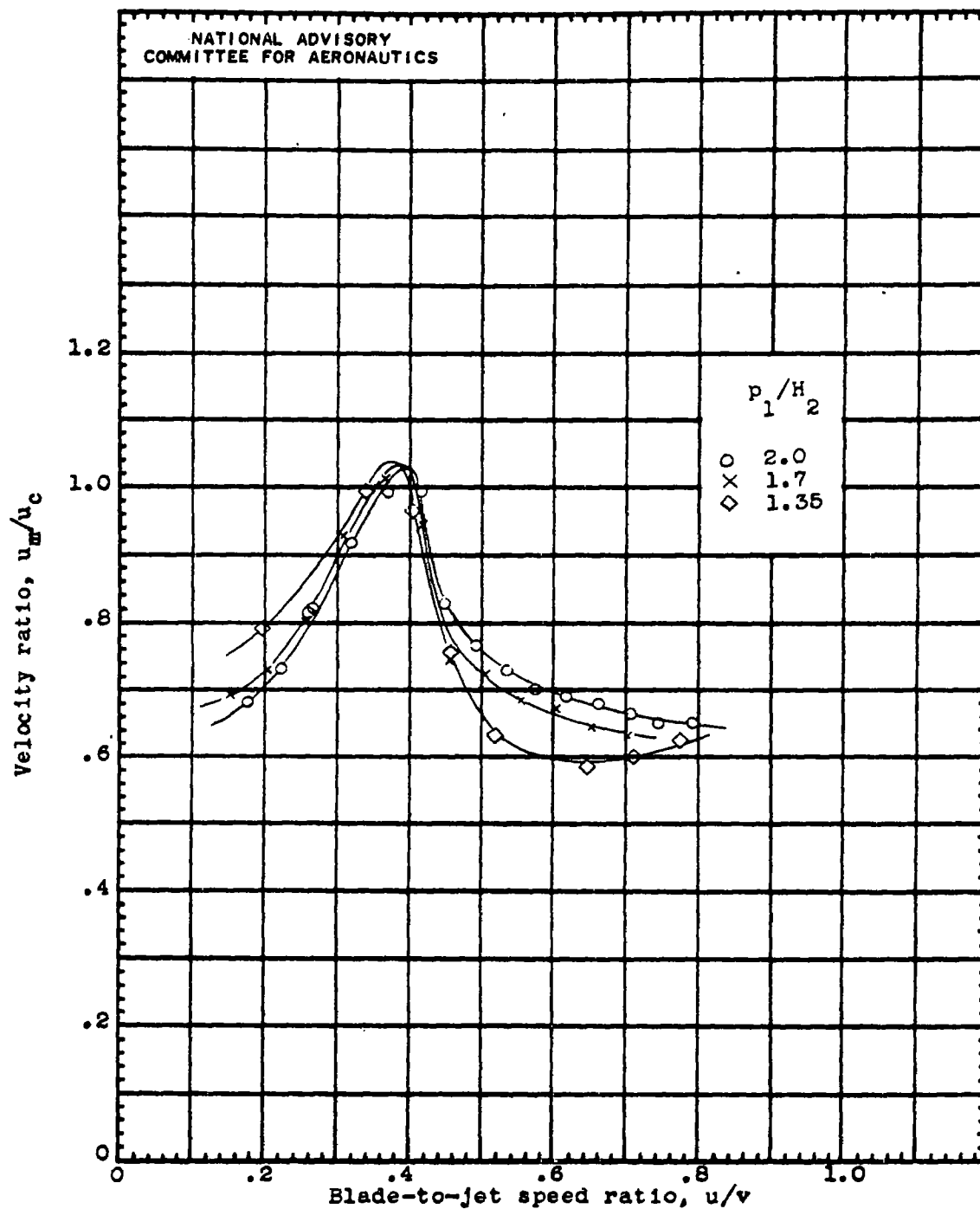
(c) Variation of ratio of effective hood-discharge
velocity to calculated hood-discharge velocity
u_m/u_c with blade-to-jet speed ratio.

Figure 8. – Concluded. Conical hood with flat cooling cap and
short-chord straightening vanes.
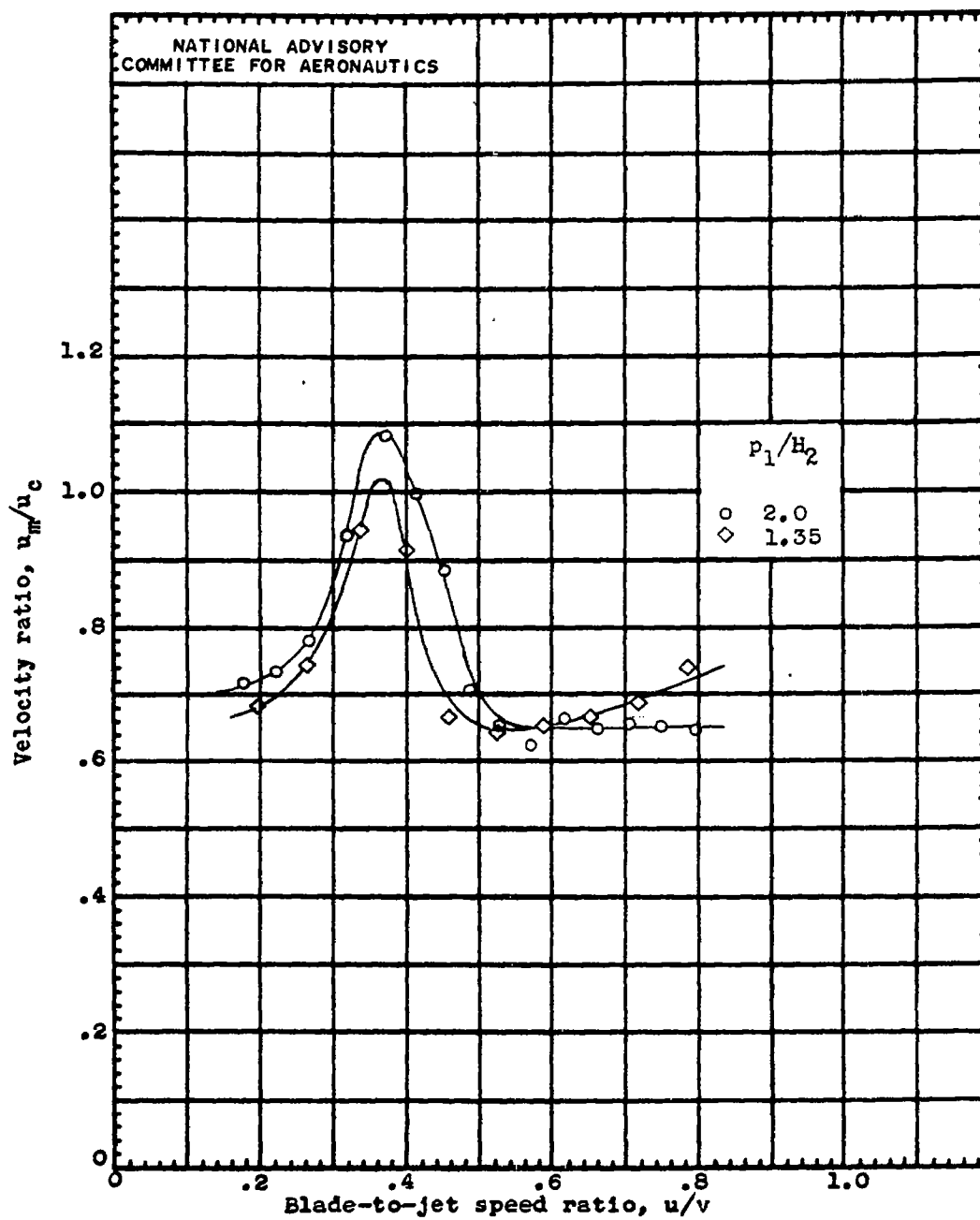
(a)   Sketch of hood.

Figure 9. - Conical hood with flat cooling cap supported by
$\frac{3}{8}$-inch tubes.

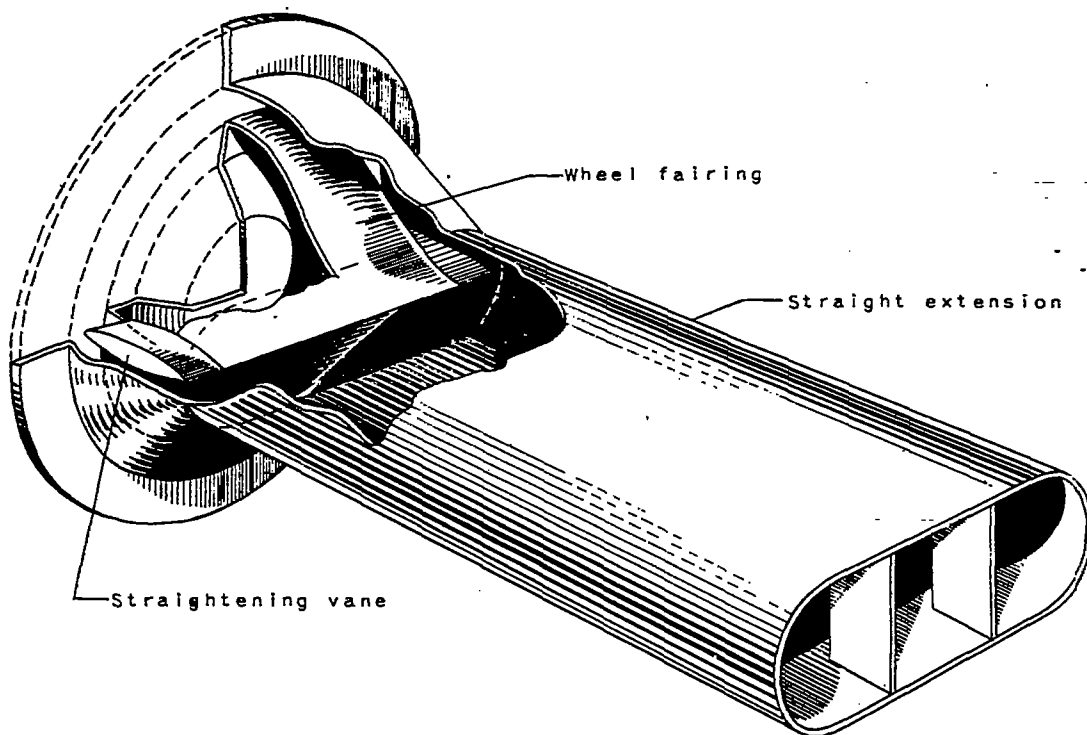(b) Variation of power and mass flow of turbine-hood
    combination with wheel-speed parameter.

Figure 9. - Continued. Conical hood with flat cooling cap
    supported by 3/8-inch tubes.
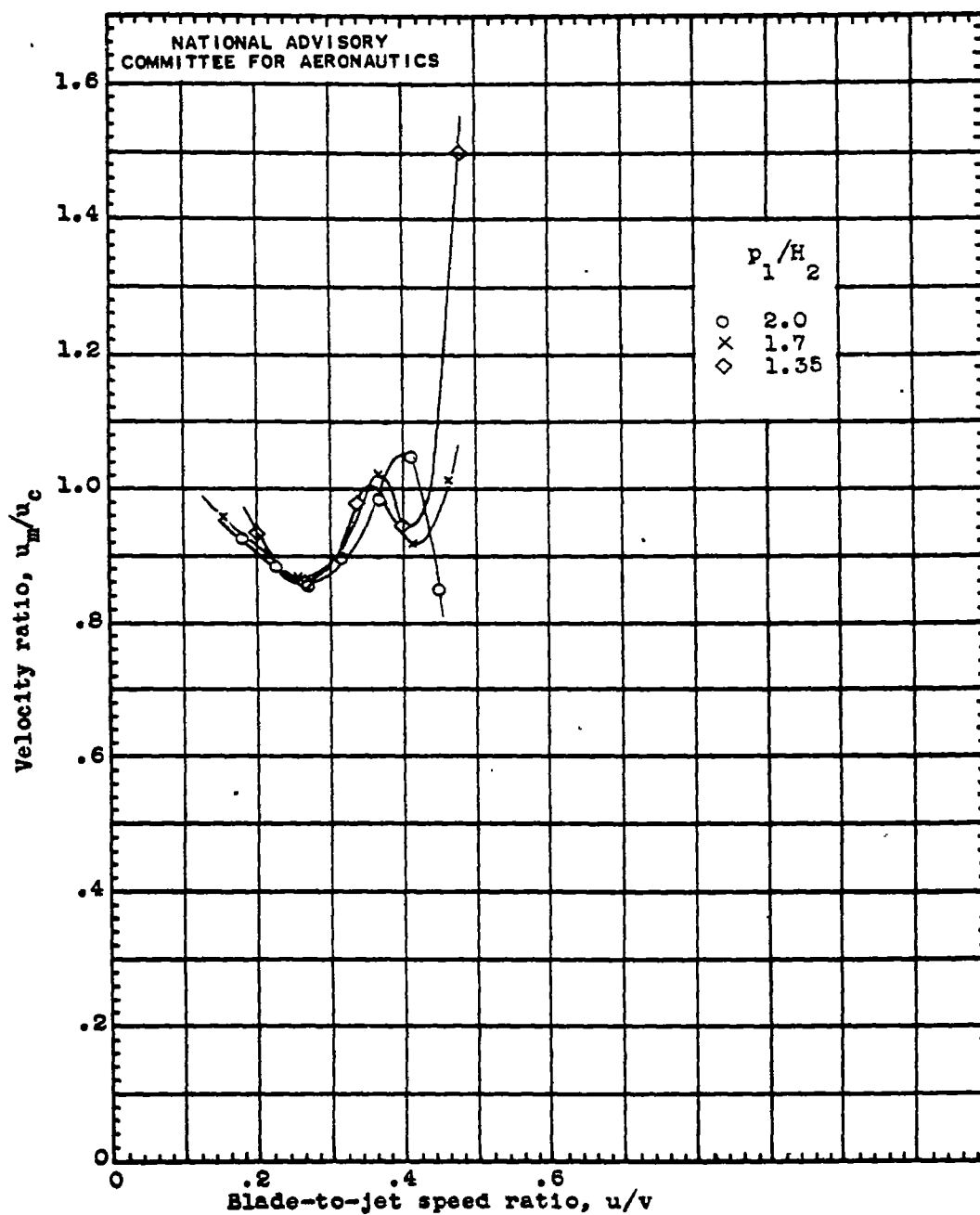
(c) Variation of ratio of effective hood-discharge
     velocity to calculated hood-discharge velocity
 u_m/u_c with blade-to-jet speed ratio.

Figure 9. - Concluded. Conical hood with flat cooling cap supported
   by 3/8-inch tubes.

Conventional cooling cap

NATIONAL ADVISORY
COMMITTEE FOR AERONAUTICS

(a)   Sketch of hood.

Figure 10. - Conical hood with conventional cooling cap.
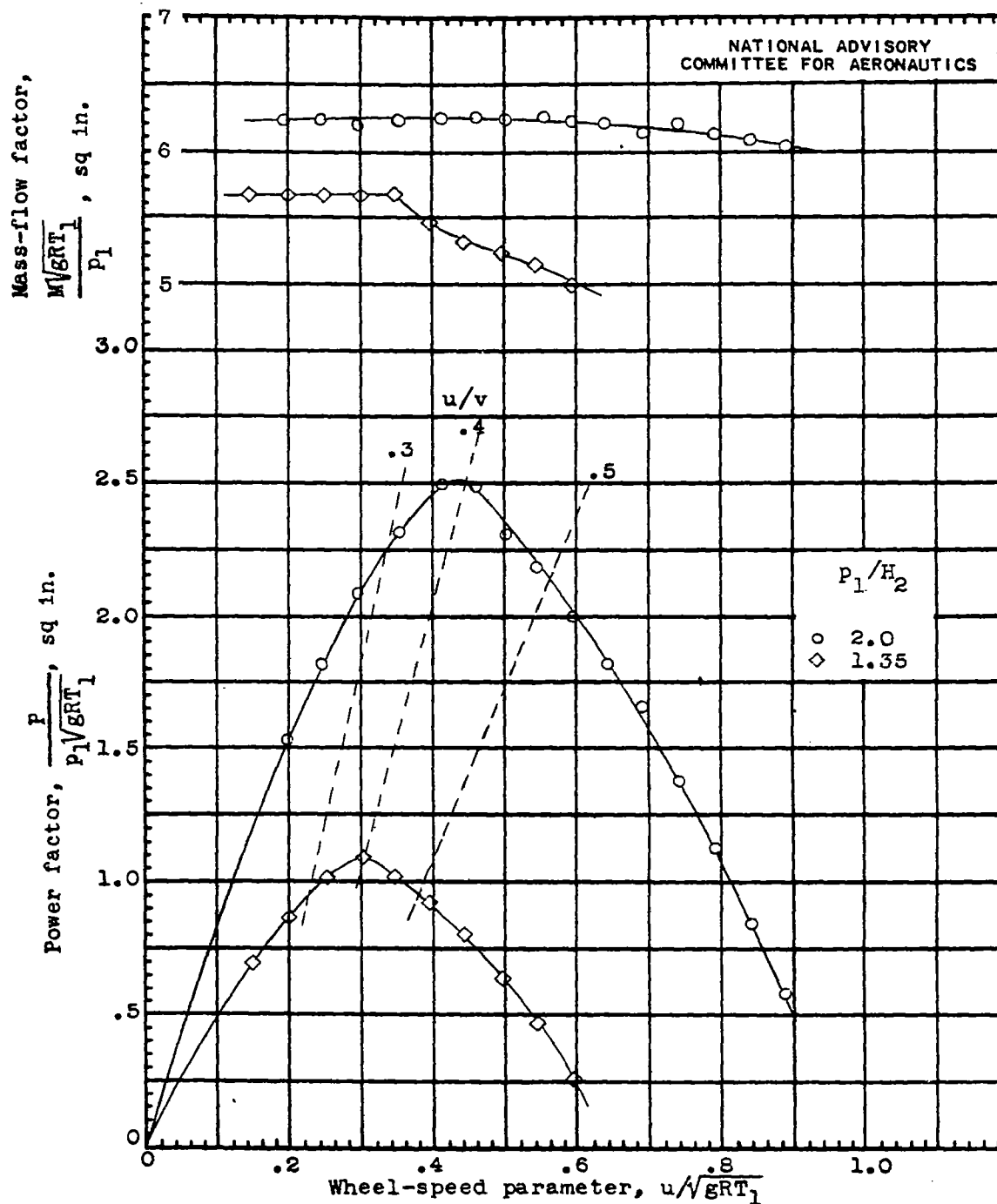
(b) Variation of power and mass flow of turbine-hood combination with wheel-speed parameter.

Figure 10. — Continued. Conical hood with conventional cooling cap.

(c) Variation of ratio of effective hood-discharge
    velocity to calculated hood-discharge velocity
    u_m/u_c with blade-to-jet speed ratio.

Figure 10. — Concluded. Conical hood with conventional cooling cap.

Wheel fairing

Straight extension

Straightening vane

(a) Sketch of hood.

**NATIONAL ADVISORY
COMMITTEE FOR AERONAUTICS**

Figure 11. – Flat-nozzle hood with straight extension.
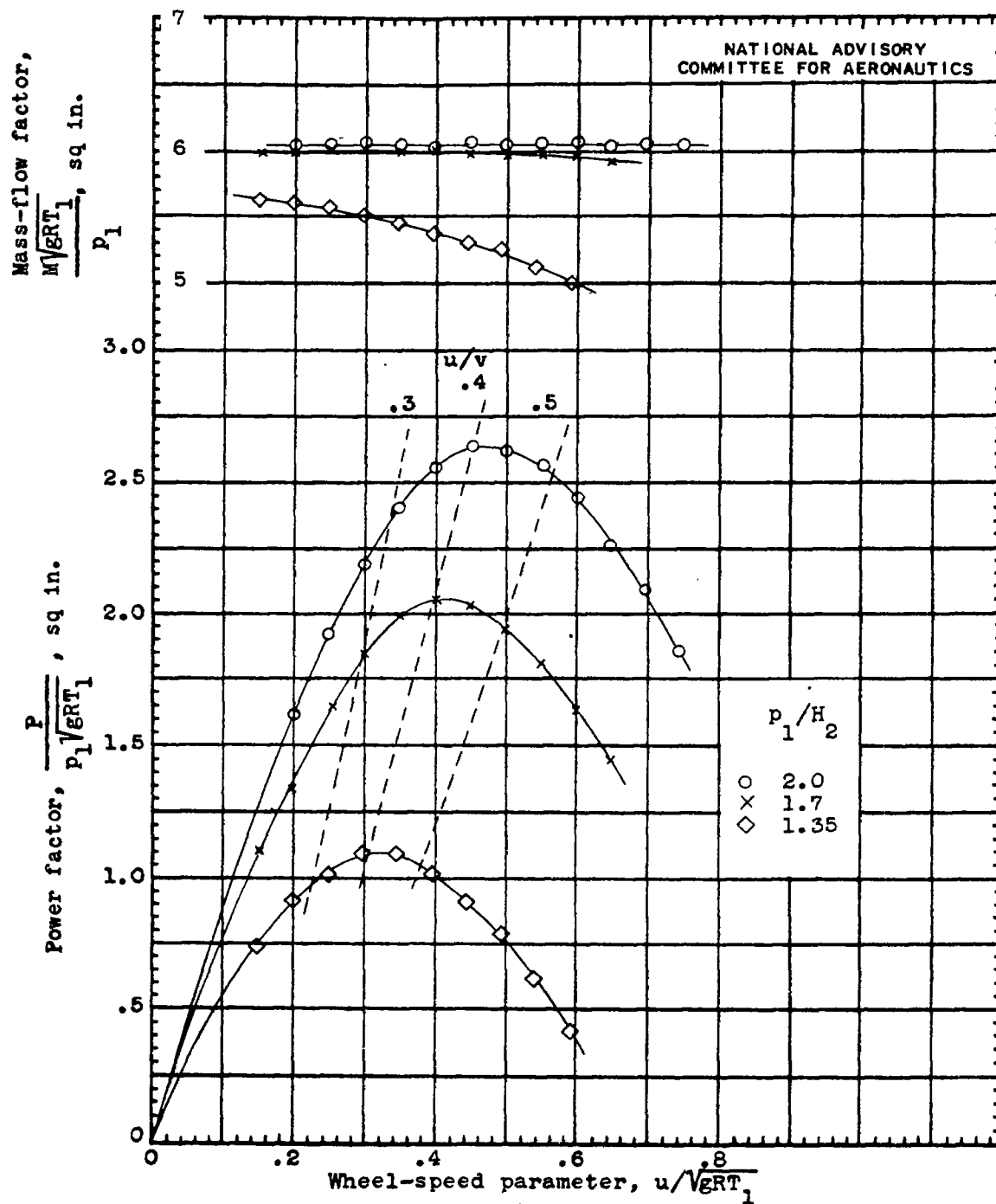
NATIONAL ADVISORY
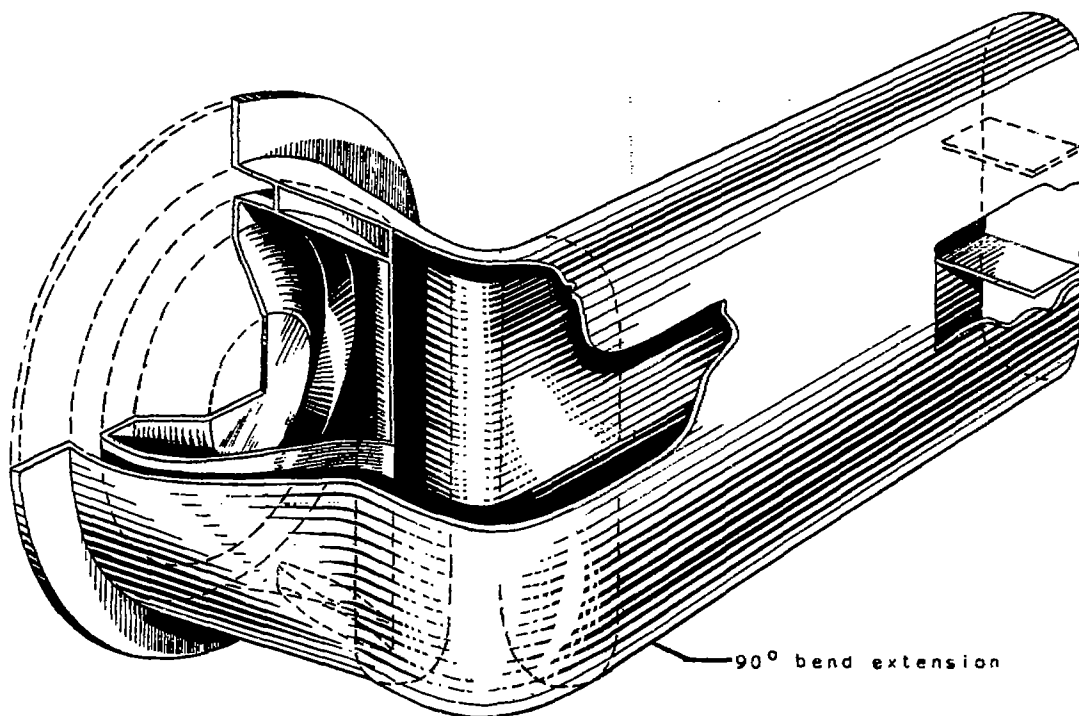COMMITTEE FOR AERONAUTICS

(b) Variation of power and mass flow of turbine-hood
combination with wheel-speed parameter.

Figure 11. — Continued.   Flat-nozzle hood with straight extension.
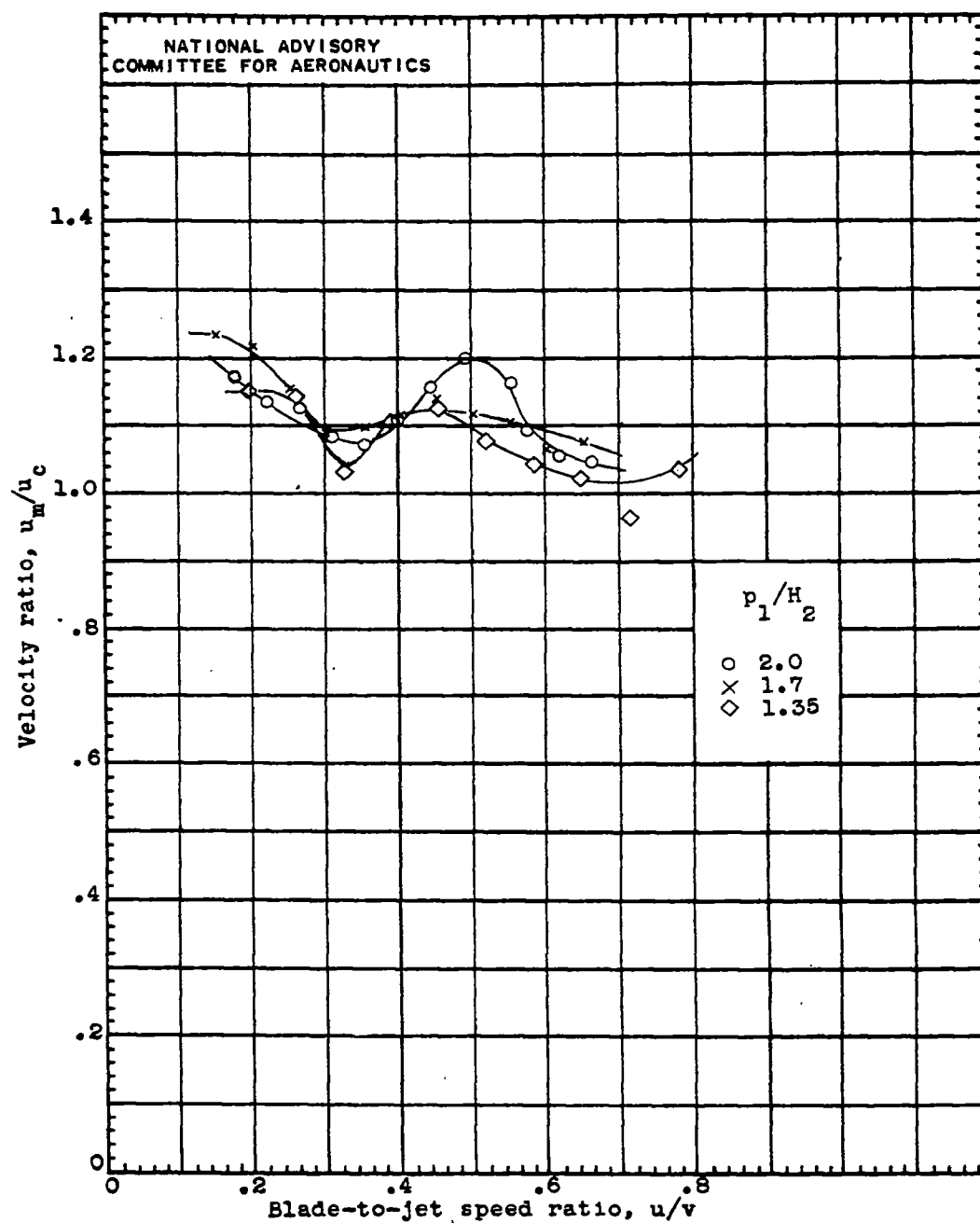
NATIONAL ADVISORY
COMMITTEE FOR AERONAUTICS

Velocity ratio, u_m/u_c

Blade-to-jet speed ratio, u/v

p_1/H_2

○ 2.0
✕ 1.7
◇ 1.35

(c) Variation of ratio of effective hood-discharge
velocity to calculated hood-discharge velocity
u_m/u_c with blade-to-jet speed ratio.

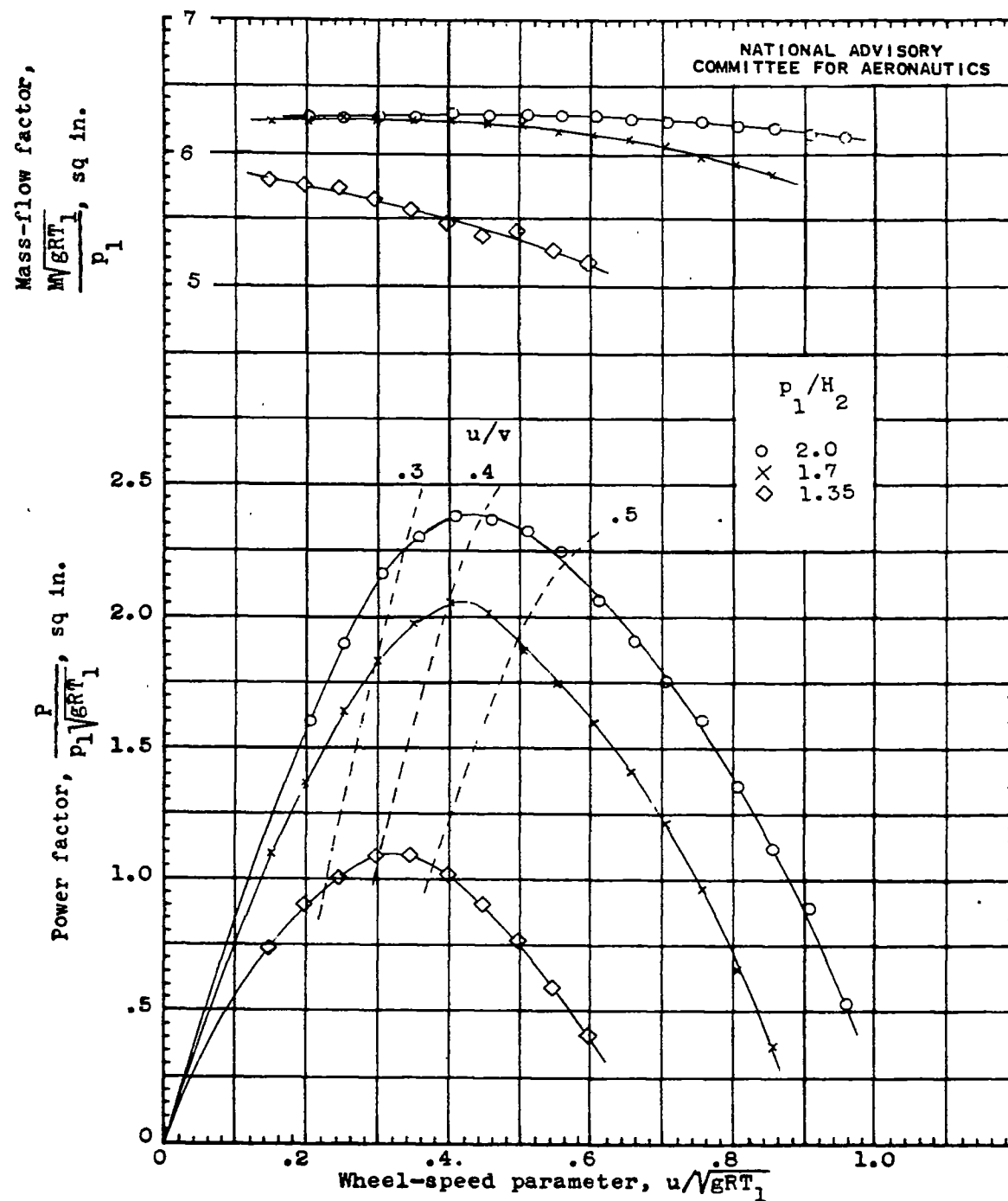Figure 11. - Concluded. Flat-nozzle hood with straight extension.

90° bend extension

**NATIONAL ADVISORY
COMMITTEE FOR AERONAUTICS**

(a)   Sketch of hood.
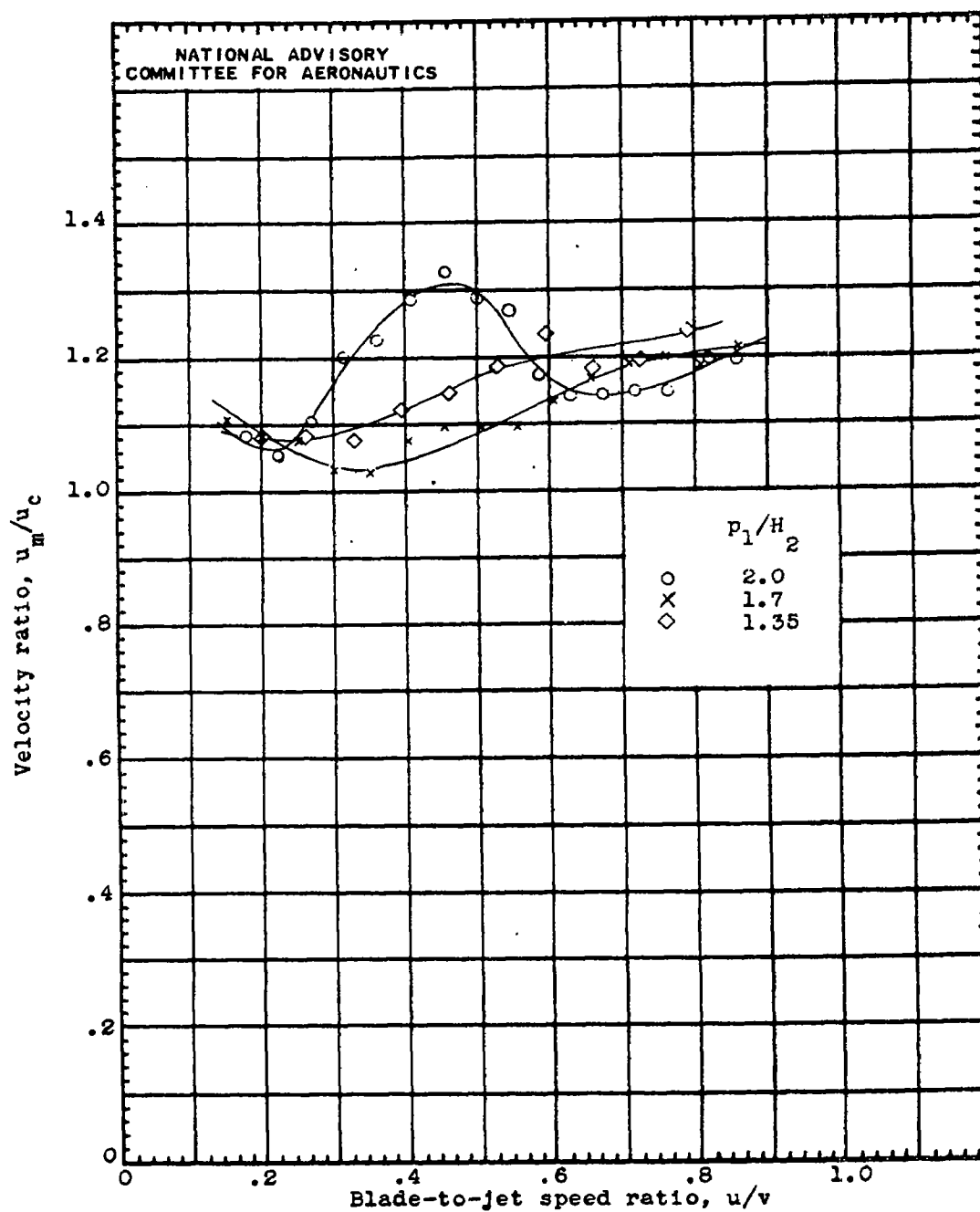
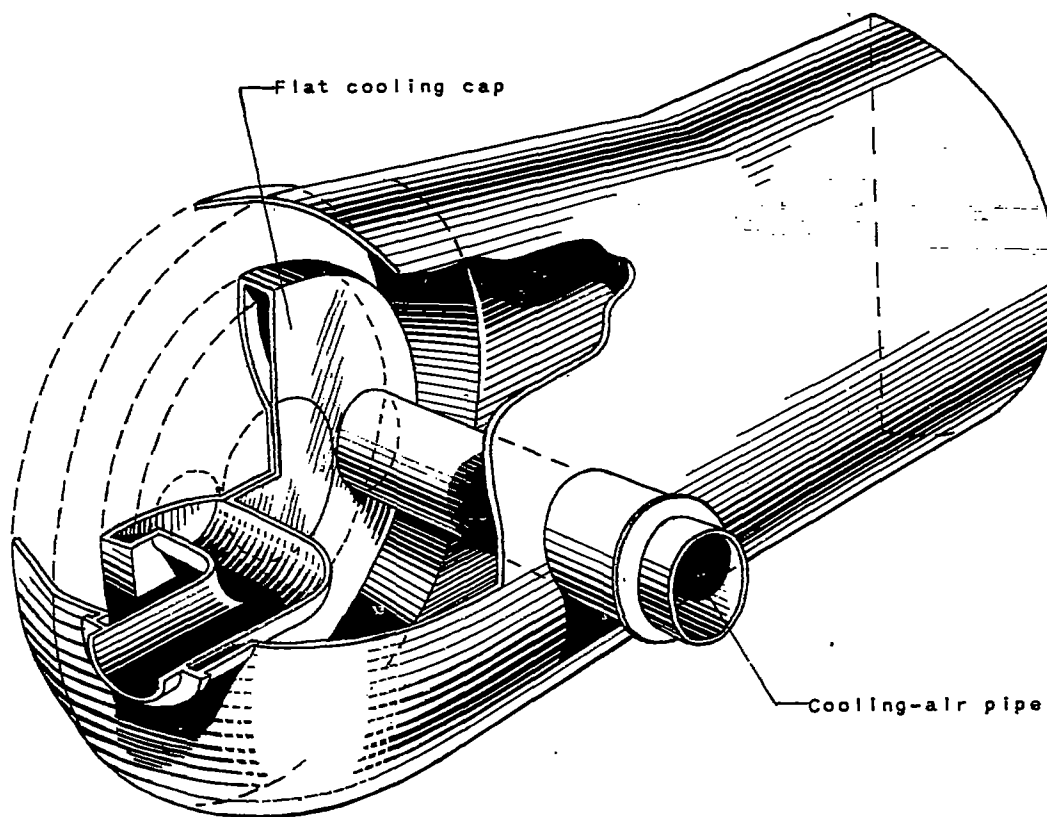Figure 12. - Flat-nozzle hood with 90° bend extension.

(b) Variation of power and mass flow of turbine-hood
combination with wheel-speed parameter.

Figure 12. — Continued.   Flat-nozzle hood with 90° bend extension.

(c)   Variation of ratio of effective hood-discharge
      velocity to calculated hood-discharge velocity
      u_m/u_c with blade-to-jet speed ratio.

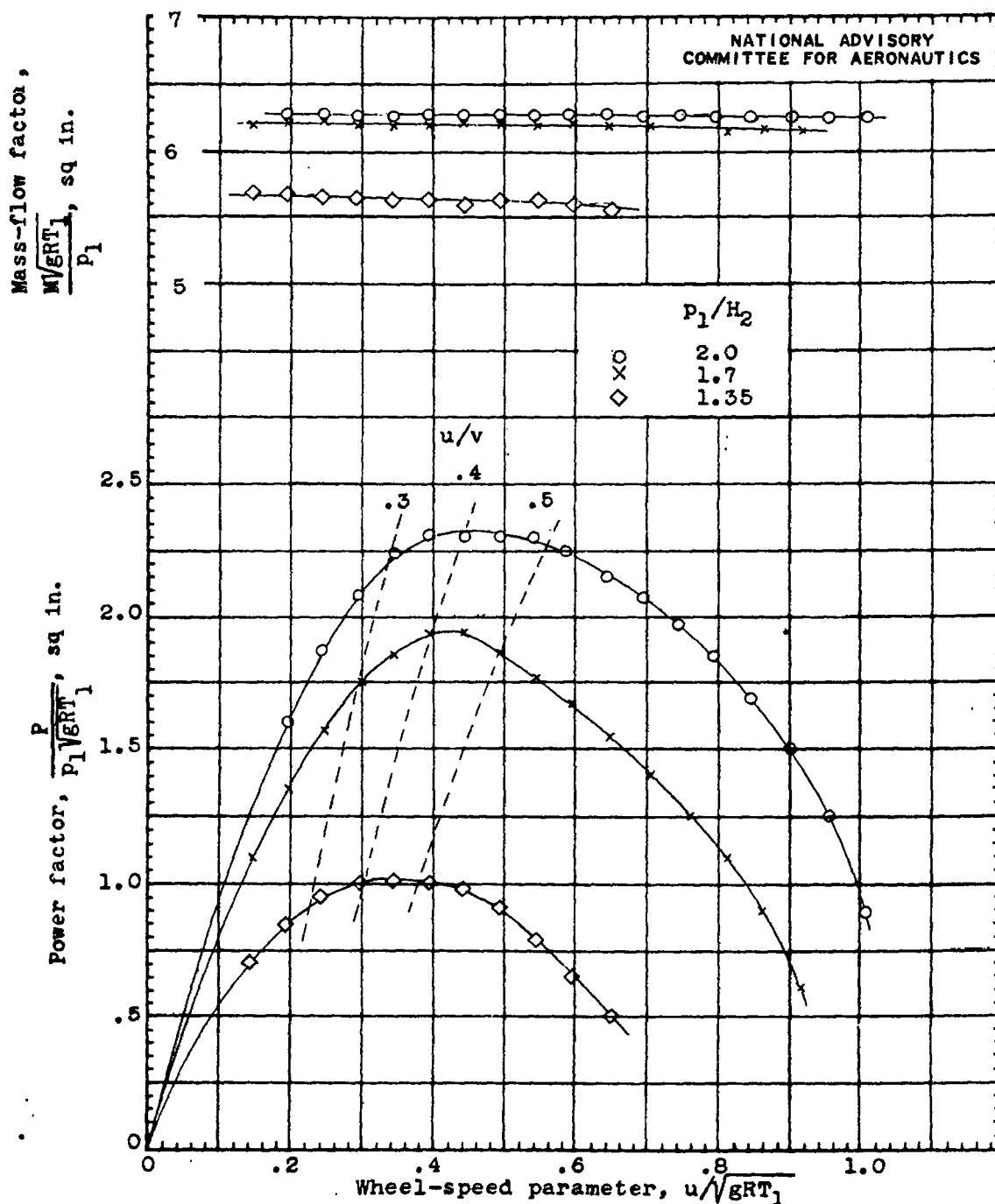Figure 12. - Concluded. Flat-nozzle hood with 90° bend extension.

Flat cooling cap

Cooling-air pipe

(a)   Sketch of hood.

Figure 13. - Short-turning-radius hood.

166-292

NATIONAL ADVISORY COMMITTEE FOR AERONAUTICS

P_1/H_2	
O	2.0
X	1.7
◇	1.35

(b) Variation of power and mass flow of turbine-hood combination with wheel-speed parameter.

Figure 13. — Continued. Short-turning-radius hood.
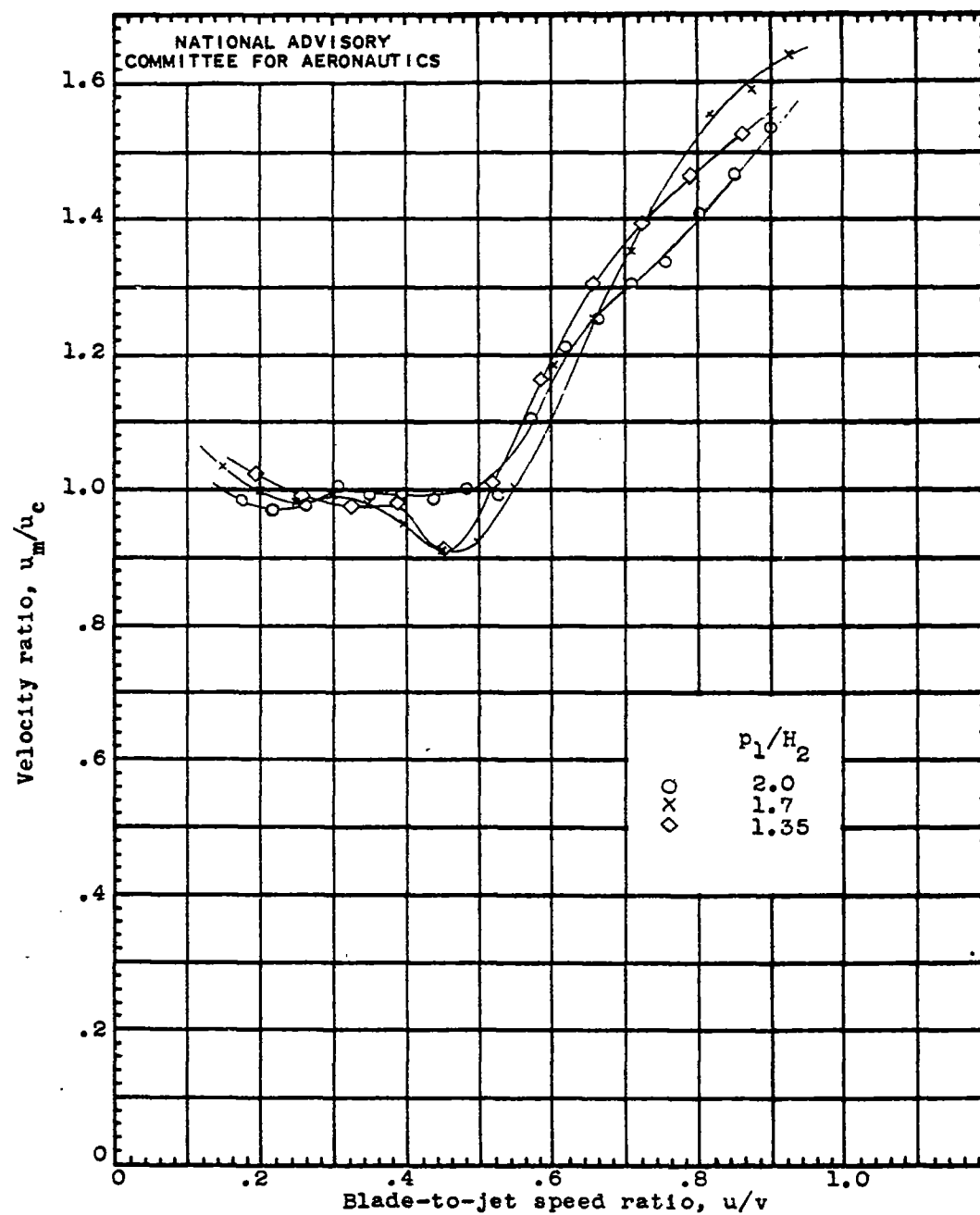
(c)   Variation of ratio of effective hood—discharge
      velocity to calculated hood—discharge velocity
      u_m/u_c with blade-to-jet speed ratio.

Figure 13. – Concluded.   Short—turning-radius hood.

Fig. 14   NACA TN No. 1149

NATIONAL ADVISORY
COMMITTEE FOR AERONAUTICS

□ Turbine without hood (fig. 3)
○ Conical hood with long-chord straightening vanes
    and hood-entrance fairing band (fig. 5)
◇ Conical hood with wheel fairing supported by
    $\frac{3}{8}$ -inch-diameter tubes (fig. 6)
▽ Conical hood with flat cooling cap and short-chord
    straightening vanes (fig. 8)
◁ Flat-nozzle hood with straight extension (fig. 11)
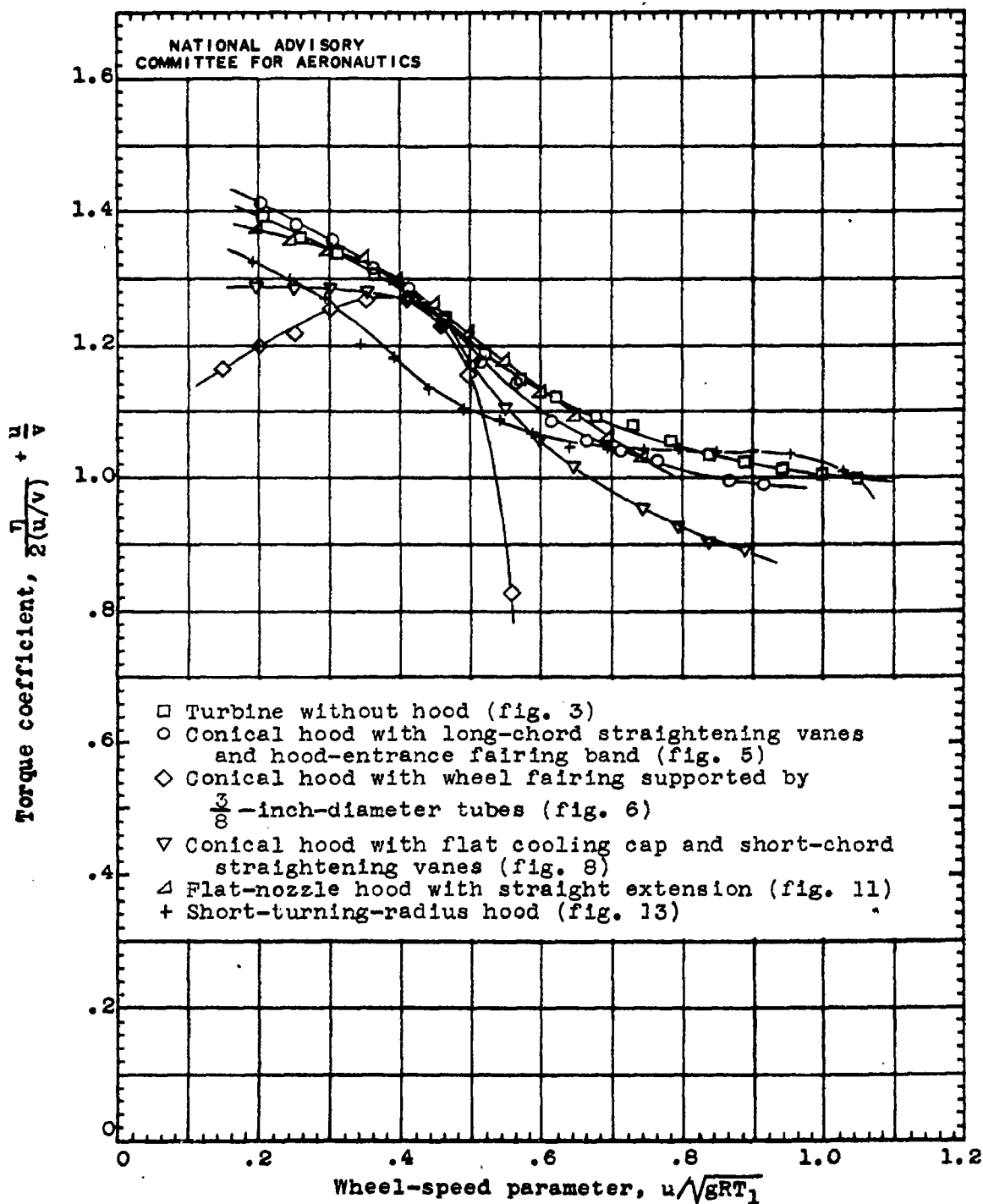+ Short-turning-radius hood (fig. 13)

Figure 14. — Relation of torque coefficient to wheel speed for
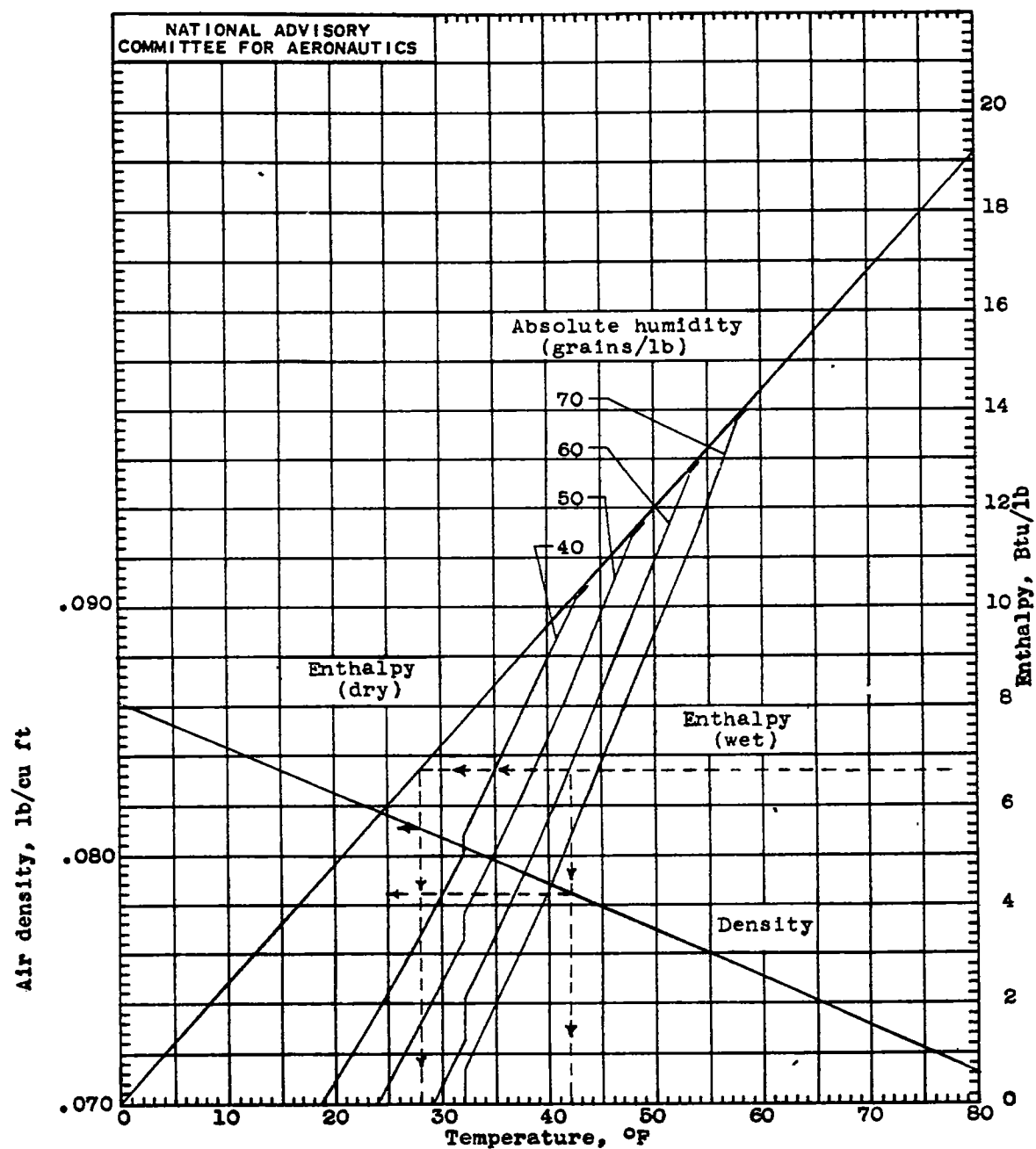various turbine-hood combinations. Pressure ratio, p_1/p_2, 2.0.

Figure 15. — Humidity-correction curve.